Quaternary Science Reviews 254 (2021) 106797

Contents lists available at ScienceDirect

Quaternary Science Reviews

journal homepage: www.elsevier.com/locate/quascirev

Century scale rainfall in the absolute Atacama Desert: Landscape response and implications for past and future rainfall

Marco Pfeiffer [a, b, *], Alexander Morgan [c, f], Arjun Heimsath [d], Teresa Jordan [e], Alan Howard [f], Ronald Amundson [a]

[a] Department of Environmental Science, Policy and Management, University of California, 130 Mulford Hall, Berkeley, CA, 94720, USA
[b] Departamento de Ingenieria y Suelos, Facultad de Ciencias Agronómicas, Universidad de Chile, Santa Rosa, 11315, La Pintana, Chile
[c] Center for Earth and Planetary Studies, Smithsonian Institution National Air and Space Museum, Washington, DC, USA
[d] School of Earth and Space Exploration, Arizona State University, ISTB4, Room 795, 781 E. Terrace Road, Tempe, AZ, 85287, USA
[e] Department of Earth and Atmospheric Sciences, Cornell University, Ithaca, NY, 14853-1504, USA
[f] Department of Environmental Sciences, University of Virginia, Charlotteswille, VA, USA

ARTICLE INFO

Article history:
Received 26 June 2020
Received in revised form
6 January 2021
Accepted 7 January 2021
Available online xxx

Handling Editor: Dr Mira Matthews

Keywords:
Soil hydrology
Rainfall threshold
Landscape response
Hyperarid soils

ABSTRACT

The Atacama Desert contains the driest regions on Earth, with significant rain occurring only a few times per century, based on sparse historical records. However, the frequency and magnitude of rainfall remains speculative. On March 24–26 of 2015, an unusual storm caused rainfall rates and quantities to exceed many historical records. Of interest is whether this storm was able to activate geomorphic processes whose impacts are evident on numerous landscape features. Here, the results of a reconnaissance from N to S transecting through the plant-free expanse of the Atacama Desert, between 22 and 26° S, are examined in relation to evidence of past runoff activity coupled with soil architecture and soil hydraulic properties. The results suggest the rain initiated some minor runoff processes on the upper hillslopes. However, the rainfall was too small to reactivate many features that appear to be driven by larger, less frequent storms. The field evidence suggests that larger scale rainfalls have occurred throughout the Quaternary, and that there are fossilized (or infrequently active) features in various stages of "repair" that provide evidence of rainfall re-occurrence. The landscapes largely escaped overland flow alteration due to the high infiltration rate capacity caused by the salt-rich soils, which we estimated to average 78 mm h^{-1} for hillslopes and 244 mm h^{-1} for alluvial soils, based on disc infiltrometer measurements. This gives a resilience, and potential rainfall threshold, to alteration by intensive rainfall events. Published paleoclimatic records coupled with evidence from soil examined at the arid/hyperarid periphery of the desert show evidence of a cessation of carbonate formation since ~11 ka, a time of aridification similar to the drying of lakes and marshlands in the hyperarid region. Thus, the past fluvial alteration features are likely to be, at least partially, remnant Pleistocene features which have been largely unaffected by Holocene events, whose magnitudes were similar to that of 2015.

1. Introduction

The hyperarid Atacama Desert of northern Chile is an ancient and profoundly dry region, yet one that bears enigmatic evidence of past rainfall that produced a variety of unusual now-fossilized features. Although less arid regions of the Atacama Desert can produce dazzling arrays of flowers following rare rainfall (Chávez et al., 2019), a large subregion of the desert from 22.6 to 26°S is almost completely devoid of plants, and is therefore an "absolute desert" (Marquet et al., 1998). This latter region is the focus of this work (Fig. 1a). The soils are rich in highly soluble salts accumulated from millions of years of atmospheric deposition (Michalski et al., 2004), yet they also contain features suggestive of partial aqueous dissolution and reorganization at multiple times in the past (Ewing et al., 2008b; Wang et al., 2015, 2016). Since the Pliocene, hillslopes have been slowly inflated by atmospheric dust and salt, yet bear surficial gravel orientation ('zebra stripes') suggestive of overland flow (Owen et al., 2013) or possibly seismic shaking (May et al.,

* Corresponding author. Department of Environmental Science, Policy and Management, University of California, 130 Mulford Hall, Berkeley, CA, 94720, USA.
E-mail address: mpfeiffer@berkeley.edu (M. Pfeiffer).

https://doi.org/10.1016/j.quascirev.2021.106797
0277-3791/

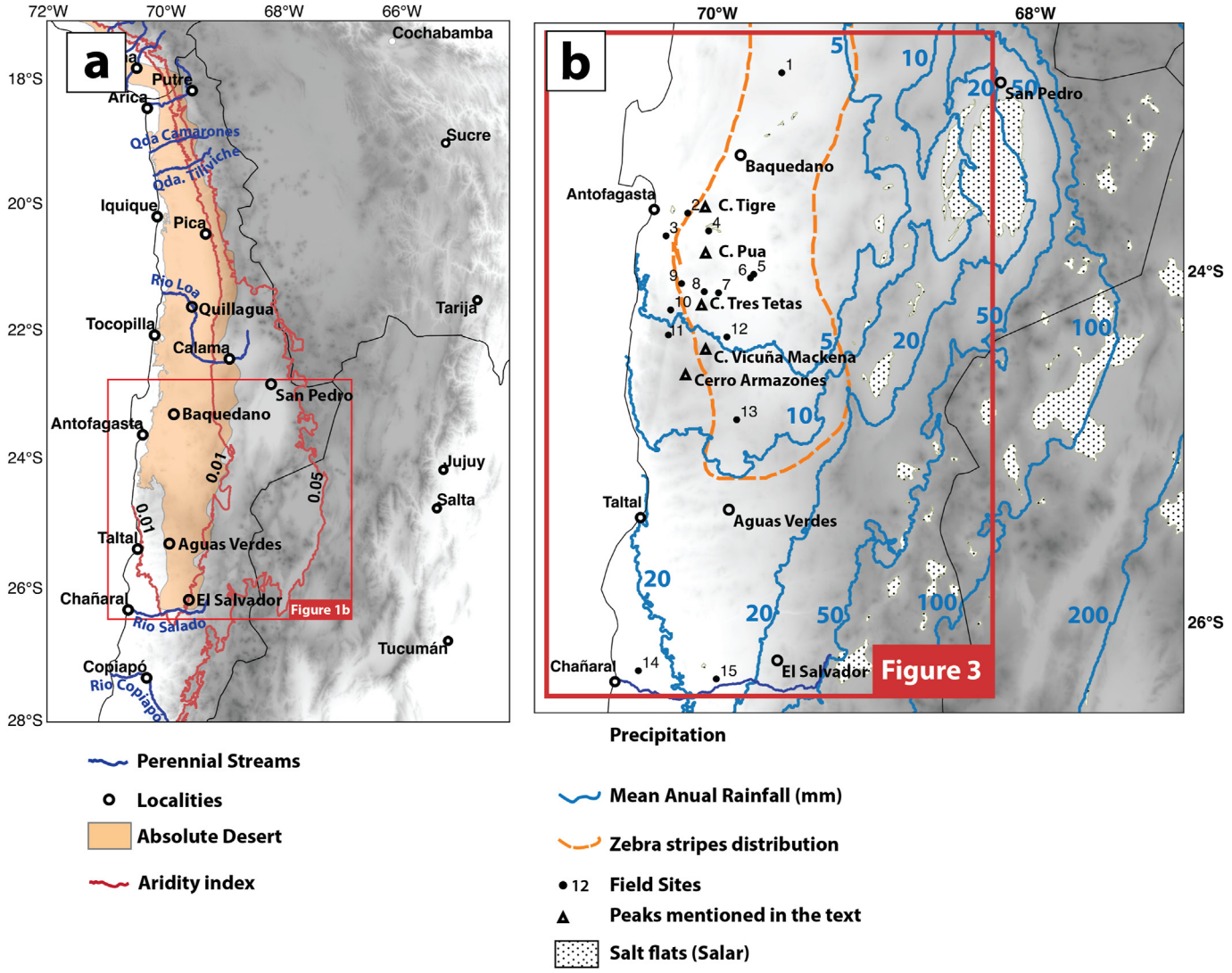

Fig. 1. (a) Map of the Atacama Desert and the adjacent regions showing the extent of the absolute desert and the isolines for aridity indexes (Precipitation/Evapotranspiration) 0.01 and 0.05, the latter corresponding to the threshold for hyperarid climates and usually used as the reference area for the Atacama Desert region. The red box corresponds to Fig. 1b, 2a and 2b. The extent of absolute desert is based on Gajardo (1994); Luebert and Pliscoff (2006); the aridity index is obtained from Zomer et al. (2008) and annual rainfall from Pliscoff et al. (2014). The hillshade background map is based on Shuttle Radar Topography Mission (SRTM) data (see Farr et al., 2007); (b) The average precipitation (in mm year $^{-1}$) for the southern Atacama Desert, the area containing "zebra stripes" on hillslopes (Owen et al., 2013), and field sites described in this study (for number correlation see also Table 1). (For interpretation of the references to color in this figure legend, the reader is referred to the Web version of this article.)

2019). Hillslopes, and colluvial and fluvial features inside the absolute desert suggest that activity occurred at specific periods of increased humidity when the amount of rain exceeded a certain threshold (Jungers et al., 2013; May et al., 2020; Medialdea et al., 2020; Ritter et al., 2019).

These features are only beginning to be recognized, and the rainfall required to initiate them is still poorly understood. Thus, the multi-day storm that impacted northern Chile in March 2015 is a unique opportunity to learn more about the desert landscape's response to rainfall, and a chance to understand more about the thresholds that must be exceeded to activate many of the unusual features in this extremely arid landscape. Here we focus particularly on how soil architecture and soil hydraulic properties influence water flow through this landscape during rainfall events. This is of particular interest as desert regions are susceptible to unpredictable geomorphological and hydrological changes when a threshold is reached (Gad-el-Hak, 2008; Goudie, 2019), and in the case of the Atacama, an increase in precipitation for 2100 is predicted due to on-going climate change (Urrutia and Vuille, 2009).

Due to a sparse population, and a relatively short duration of settlement, long-term records of precipitation are rare (Schween et al., 2019). Only one other large historical storm, which occurred in 1991 in Antofagasta, has rainfall rate data (Garreaud and Rutllant, 1996; Vargas et al., 2006). The March 24 and 26, 2015 storm caused high rainfall across parts of the southern Atacama desert (Barrett et al., 2016; Bozkurt et al., 2016; Jordan et al., 2019; Rondanelli et al., 2019; Scott et al., 2017). Major stream and river channels, some of which seldom carry surface water, became active and led to significant destruction. Particularly devastating was the flooding of the Salado and Copiapó Rivers at the southern border of the desert (Cabré et al., 2020; Valdés-Pineda et al., 2017; Wilcox et al., 2016). It appears that much of the water that activated these drainages occurred from precipitation at relatively high elevations (above ~2800 m.a.s.l.), outside of what is considered the 'absolute desert'. Within the desert, there was little runoff into

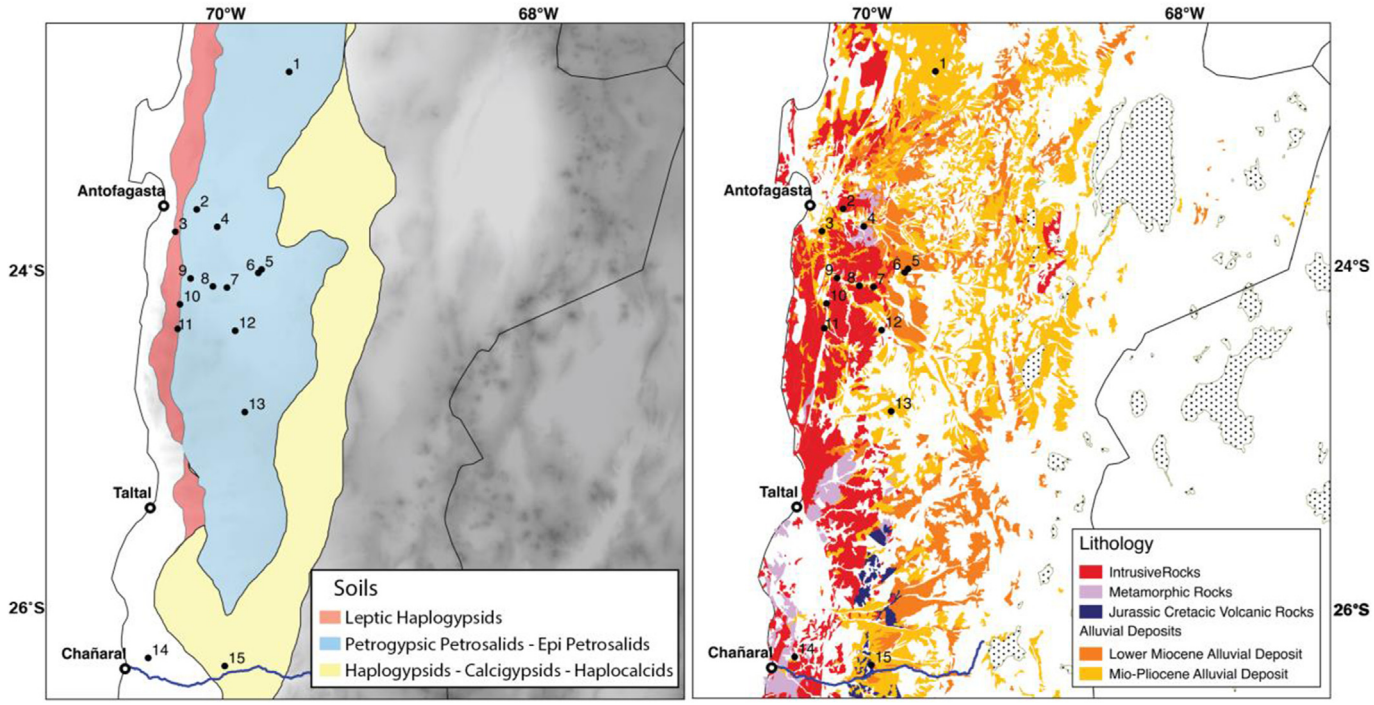

Fig. 2. a) Soil distribution at the Sub-Group level for the absolute desert of the Atacama based on Diaz and Wright (1965). The hillshade background map is derived from Shuttle Radar Topography Mission (SRTM) data (see Farr et al., 2007) and b) main lithological units for the area of interest in this study (from SERNAGEOMIN, S. N. d. G. y. M., 2003). The numbered black dots correspond to study sites mentioned in Table 1.

tributaries of local drainage systems (Jordan et al., 2015). While recent studies focused on the storm impact on streamflow (Jordan et al., 2015) and the use of remote sensing tools to capture soil moisture and surface erosion (Jordan et al., 2020; Scott et al., 2017), there is still a lack of knowledge on how soil specifically in this area has reacted to this rainfall.

2. The absolute desert

2.1. Geographical setting

The Atacama Desert is located between 18° S and 27° S, within a tectonically active forearc with four major parallel (N–S) morphotectonic units. These units are (from west to east): the Coastal Cordillera; the Central Depression; the Precordillera and the Western Andean Cordillera. The Central Depression, the focus here, is a ~50 km wide continental basin, and is filled with Palaeogene-Neogene alluvial, fluvial and evaporitic deposits mainly derived from the Precordillera and Western Andean Cordillera. It is interrupted by a series of local ranges and small mountains. This study focuses on sites in the Central Depression between 22.6 and 26° S at elevations from 500 to 2100 m.a.s.l. To the east lies the Precordillera and Western Andean Cordillera, where precipitation increases with elevation (Fig. 1b), and sparse plants are widespread.

The Mean annual precipitation averages <5 mm/year, with a steep latitudinal and elevational gradient (Fig. 1b). The record of humid periods during the Quaternary is largely derived from the desert borders (Betancourt et al., 2000; de Porras et al., 2017; Latorre et al., 2002), or from streamflow and wetland activation related to recharge that occurred in the Andes (Díaz et al., 2012; Gayo et al., 2012; Nester et al., 2007; Pfeiffer et al., 2018). Few studies have documented the history of changes of precipitation within the absolute desert. Some information is provided by the chronology of salic soils (Jordan et al., 2014), sedimentary sequences (Diederich et al., 2020; Ritter et al., 2019) and hillslope erosion (May et al., 2020; Medialdea et al., 2020). A small closed drainage basin, with no surface water or groundwater connection to Andean catchments, has recorded precipitation variation with high temporal resolution over the last 225,000 years (Ritter et al., 2019).

The study area is dominated by alluvial deposits of pre-Pleistocene origin (Marinovic et al., 1995; SERNAGEOMIN, S. N. d. G. y. M., 2003). These contain complex soils that suggest multiple stages of formation (Amundson et al., 2012a). These deposits are partly deeply incised along major drainages, or buried by younger deposits from the Mio-Pliocene age along mountain fronts. Amundson et al. (2012b) suggested that hillslopes were mantled with silicate soils under an arid to semi-arid climate up until the late Pliocene, and were then stripped by erosion. The slopes have subsequently slowly accumulated dust, salt, and local sources of colluvial material (Owen et al., 2013). All alluvial deposits from the Pleistocene age or older have significant accumulations of salt and dust (Ewing et al., 2006; Owen et al., 2013). The area containing sulfate and nitrate-rich soils (Petrogypsid petrosalids; Fig. 2a) is restricted to the hyperarid desert (Finstad et al., 2014; Placzek et al., 2010). These soluble salts imply a prolonged interval incapable of dissolving and removing them. Amundson et al. (2012b) calculated a stream incision of 1.1 m during the Quaternary, about ten times less than during the Mio-Pliocene period, suggesting a decline of ~100 mm yr^{-1} in rainfall.

Despite the prolonged aridity, surficial features suggest episodes of increased rainfall during the Quaternary. Those episodes are necessary for the redistribution of salts over depths of 3 m in the soil (Ewing et al., 2006, 2008b). Past fluvial activity is evident in deposits of a small endorheic basin (Ritter et al., 2019), erosion/deposition cycles (Jungers et al., 2013), hillslope zebra (stone)

stripes, rills and colluvial deposits on hillslopes (Amundson et al., 2012b; Medialdea et al., 2020; Owen et al., 2013), and the presence of pipes that run sub-horizontally below the soil surface (Amundson et al., 2012b).

2.2. Historical rainfall and the March 2015 storm

Rainfall in the Atacama Desert has decadal return intervals, while in the adjacent Andes rainfall is more frequent (Houston, 2006b). Precipitation records covering the last 100 years exist only for cities on the Coast (Arica, Iquique and Antofagasta), while data for the interior spans only a few decades (Fig. S1). Ortlieb (1995) compiled anecdotal information together with instrumental records for the period between 1796 and 1992. In the Pampa del Tamarugal region (19.5° - 21° S), only one rainfall (1882) was recorded in the 19th century (near the coastal city of Iquique) and two significant rainfalls in the Pampa del Tamarugal occurred in the 20th Century (in 1911 and 1965). In the 20th century, coastal Antofagasta had four heavy rainfalls (20–40 mm/3h) which caused debris flows. The two largest occurred in June 1940 (39 mm total) and June 1991 (42 mm total) (Vargas et al., 2006). The June 18, 1991 rainfall had an average rate of 5–14 mm/h, with a maximum of up to 24 mm/h, which was considered a "hundred-year" rainfall at the time (Garreaud and Rutllant, 1996). The 1991 rain was caused by a winter cold front that migrated northward. This also impacted the interior desert, causing precipitation in Baquedano (17.5 mm) and Aguas Verdes (33.5 mm). However, the 1991 front did not reach Quillagua, Calama and San Pedro de Atacama to the north and east (Fig. 1a).

In light of this history, rainfall quantities like those that occurred in the March 24–26, 2015 storm appear to occur once or twice per century but are commonly more localized and less widespread than the 2015 event. Historical floods, debris and mudflows in the region are mostly associated with rainfall that occurs in the Andean Precordillera and Cordillera such as the Great Atacama floods of 2001 in the Loa river basin (Houston, 2006a), flash floods in 2000, and mud/debris-flows in 2012 at the Pampa del Tamarugal (Houston, 2002; Morgan et al., 2014; Sepúlveda et al., 2014). During these events, rainfall did not occur in the absolute desert or at least was not recorded.

Fig. 3 shows the extent of the 2015 rain, which was due to an eastward moving cutoff low that coincided with unusually high air moisture of tropical origin generated by positive sea surface temperature anomalies over the eastern tropical Pacific Ocean (Barrett et al., 2016; Bozkurt et al., 2016). The storm began in the afternoon of March 24th and ended in the early morning of the 27th, with the heaviest precipitation occurring between 24° to 28° S (Bozkurt et al., 2016; Jordan et al., 2019). El Salvador had the highest amount of 90 mm (2240 m a.s.l. elevation, 26.2° S), followed by Aguas Verdes with 85 mm (1637 m a.s.l., 25.4°S) (see Fig. 1 for locations). Taltal had rates between 0.7 and 10.7 mm/h, with a few periods that reached up to 48 mm/h (www.meteochile.cl) (Fig. S2). Rain occurred in the inland desert below 2000 m a.s.l. (Bozkurt et al., 2016). TRMM data and station data show both a first-order eastward increase in precipitation as well as a second-order SE-trend to heterogeneity in total precipitation for the storm (Fig. 3b and d). Modeled precipitation from Bozkurt et al. (2016) suggests a high degree of heterogeneity, with the highest precipitation rates just east of Antofagasta and a broad southeastern region at elevations above 2000 m a.s.l. between 25 and 26° S (Fig. 3).

Ephemeral stream channels became active (Jordan et al., 2015). The stream response, debris flows, and soil moisture evolution have been reported (Jordan et al., 2020; Tapia et al., 2015; Valdés-Pineda et al., 2017; Wilcox et al., 2016). Scott et al. (2017) showed that the precipitation caused a spatially variable and transient soil moisture response, and that the land surface of most landforms returned to their original spectral conditions after a few months.

3. Methods

3.1. Study locations and rainfall data

The first field observations were conducted within two weeks of the 2015 rain, traversing an elevation gradient from the coast to the Pre-Andean front range. More intensive field work was conducted in January 2016, focusing on areas that received significant rainfall based on the (Tropical Rainfall Measuring Mission) TRMM data model (Iguchi et al., 2000). Fifteen sites were examined along a 400 km N–S transect between 23° to 25° S. With one exception, the sites were all in the hyperarid dust and salt accumulation zone (Fig. 2). Site 14, near Chañaral, was outside the sulfate accumulation zone (Fig. 2; Table 1).

Model-derived precipitation from Bozkurt et al. (2016) more closely reflected local rain gauge data than TRMM estimates (Jordan et al., 2015). However, for precipitation rates, TRMM has a higher time step resolution (0.5 h) than the data obtained from Bozkurt et al. (2016) (3 h time step). Historical and event rainfall data were examined from 8 stations (Fig. S1). Event total rainfall and rainfall intensity was available for the Taltal rainfall station at a frequency of 1 min (Fig. S2).

The area studied lacks any stream monitors, except for the Loa river which is located about 50 km north of our observation area. Because of this, the observations on the level of landscape activation was mainly based on landscape features that account for changes due to water flow and/or precipitation. In this sense, we can mention the following features as signals of water flow: the presence/absence of fresh deposits (the desert seemed to cover them quickly with salts and dust), change in the color on hillslopes, rills cutting zebra stripes and water marks in channels on which we conducted hydrological measurements (See Tables S1 and S2 for further details).

The same area was analyzed by Scott et al. (2017), using the InSAR technique discriminates between parts of the landscape that experienced sufficient overland flow or channelized flow to transport sediment during March 2015, and those that did not. The radar coherence indicates that only a small subset of channels were activated. According to their data, sites 12 and 13 experienced too little overland or channelized flow to cause erosion or transport of sediment, whereas sites 10 and 11 likely experienced erosion or deposition.

Additionally, we complemented this information using satellite imagery where available in order to evaluate the occurrence of overland and stream flow as well as flash floods (See Supplementary Materials).

3.2. Soil properties

We described soil profiles along channel walls, road cuts, and excavated trenches. At the Yungay alluvial fan (site 7b), the topsoil of a 4 m^2 parcel was removed in different steps using an air gun attached to a compressor. We recorded polygon size, cracks and differences in material density and composition, complementing soil observations previously reported by Ewing et al. (2006) for the same site.

Undisturbed blocks (~15 cm width) of the upper 30 cm of the $CaSO_4$ layer at Oficina Americana, Yungay and Barazarte (Sites 5, 7b and 9) were removed, as was the sand that filled cracks (up to 60 cm) at Yungay. Additionally, undisturbed samples of the

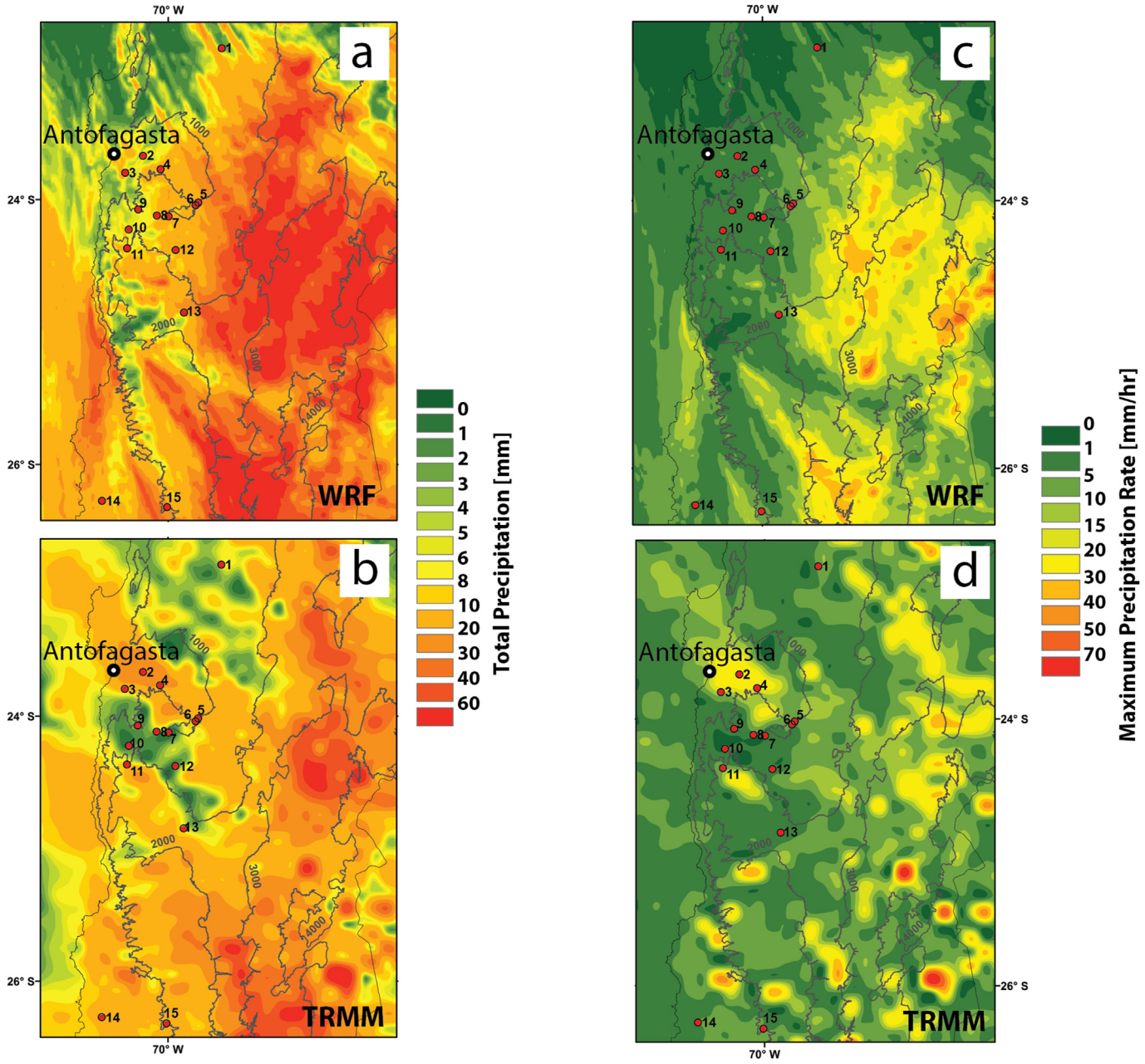

Fig. 3. Three day (24–26 March 2015) accumulated rainfall (mm) according to (a) model estimates (Bozkurt et al., 2016) and (b) TRMM data. Maximum rainfall rates (mm hr^{-1}) obtained from (c) Bozkurt et al. (2016) and (d) TRMM data. The spatial resolution of modeled data (a and c) is 2 × 2km per pixel, and 25 × 25 km per pixel for TRMM (b and d). Temporal resolution is 3 h for (c) and 0.5 h for (d). Elevation contour lines are in grey. The numbered Red dots correspond to field observed locations mentioned in Table 1. The contour lines are based on Shuttle Radar Topography Mission (SRTM) data. (For interpretation of the references to color in this figure legend, the reader is referred to the Web version of this article.)

uppermost sulfate layer were carefully packed in Saran polymer resin and then the volume was determined through water displacement (Brasher et al., 1966). Samples were placed in a ceramic plate connected to a tube with water, and water retention was measured using the hanging water column method, which is the most appropriate for low suction ranges in highly porous materials (Dane and Hopmans, 2002). For each sample, the drying curve was replicated three times. Laboratory measures were used to fit the Van Genuchten (1980) function for the Soil Water Characteristic curve using the RETC computer program (Van Genuchten et al., 1991). Water retention values were used in the equations to estimate the soil water fluxes reported in section 4.3.

Ten HOBO Prov2 (U23-002) relative humidity (RH) and temperature sensors were installed along a soil depth profile at Yungay (site 7b) in August 2015. An 80 cm deep trench was dug, and a drill was used to place sensors at depths of 1, 5, 10, 20, 30, 40, 50, 60, 70 and 80 cm in the trench wall. Sensors were placed 15 cm from the trench wall in the soil and backfilled with soil to isolate them from the open trench to record the soil microclimate. Upon refilling, soil RH and temperature values were obtained at 30 minute intervals. RH and temperature measurements were used to simulate water vapor flux between different soil depths based on Fick's law (Fick, 1855). For details of water content and flux estimation methods, see supplementary material.

Table 1
Field sites locations main features.

Site N°	Site Name	Location	Elevation [m a.s.l.]	MAP [mm]	MAT [°C]	Geomorphology	Geology	Soil type (Soil zone according to map in Fig. 2)
1	Oficina Pedro de Valdivia	22.856°S, 69.5959°E	1486	<1	16	Incised alluvial fan	Mio Pliocene Alluvial Deposit	Petrogypsic Petrosalid
2	Subestación O'Higgins	23.6669°S, 70.1869°W	761	2	16	Hillslope	Jurassic Intrusive (Diorite)	Petrogypsic Petrosalid
3	La Negra	23.8007°S, 70.3280°W	500	3	16	Incised alluvial fan-Pediment	Mio Pliocene Alluvial deposit	Leptic Haplogypsid
4	Lomas Negras	23.7710°S, 70.0541°W	690	2	17	Hillslope	Metamoprhic Rocks (Sierra del Tigre Formation -Devonian-Carboniferous)	Petrogypsic Petrosalid
5	Oficina Americana	24.0255°S, 69.7734°W	1019	3	17	Incised alluvial fan	Lower Miocene Alluvial deposit.	Petrogypsic Petrosalid
6	Oficina Yugoslavia	24.0390°S, 69.7917°W	990	3	17	Incised alluvial fan	Mio Pliocene Alluvial Deposit	Petrogypsic Petrosalid
7	Yungay	24.1098°S, 70.0144°W	1028	4	15	Hillslope (7a)-Incised alluvial fan (7b)	Mio-Pliocene alluvial deposit and Jurassic Intrusive (Granodiorite)	Petrogypsic Petrosalid
8	Laguna Seca	24.1188°S, 70.0833°W	1125	4	15	Hillslope	Jurassic Intrusice (Granodiorite)	Petrogypsic Petrosalid
9	Barazarte	24.0720°S, 70.2263°W	1015	4	15	Hillslope	Jurassic Intrusive (Diorites-Gabro).	Petrogypsic Petrosalid
10	Paranal	24.2229°S, 70.2940°W	1592	4	12	Hilslope-Fault Scarp	Volcanic Rocks from La Negra Formation (Jurassic)	Leptic Haplogypsid
11	Pampa Remiendos	24.3671°S, 70.3085°W	2162	6	11	Hillslope-Fault Scarp	Jurassic Intrussive Rocks (Gabro-Diorite)	Leptic Haplogypsid
12	Oficina Rosario	24.3797°S, 69.9427°W	2144	4	15	Hillslope	Cretaceous Intrusive (Granite).	Petrogypsic Petrosalid
13	Pampa Grande	24.8520°S, 69.8763°W	2147	8	12	Incised alluvial fan	Mio-Pliocene Alluvial deposits.	Petrogypsic Petrosalid
14	Chañaral Hillslope	26.2716°S, 70.5011°W	580	24	17	Hillslope	Triassic Intrusive (Monzogranite)	Lithic Torriorthent
15	Pueblo Hundido	26.3220°S, 70.0080°W	1098	17	17	Hillslope	Jurassic Volcanic rocks.	Calcigypsid

MAP and MAT: Pliscoff et al. (2014) full raster is downloable at http://www.unil.ch/ecospat/page89413.html. Geological information is from SERNAGEOMIN, S. N. d. G. y. M., 2003. Soil type distribution is based mainly in the work of Diaz and Wright (1965).

We collected samples of the upper 30 cm of the $CaSO_4$ layer at the Americana, Yungay, Barazarte, and Oficina Rosario sites (Sites 5, 7b, 9, 12). At Pedro de Valdivia, Yungay, Laguna Seca and Oficina Rosario (Sites 1, 7b, 8, 12), efflorescences on the desert crust or recent channel walls were collected. X-ray diffraction (XRD) was performed on whole samples with a PANalytical X'Pert Pro diffractometer at 40 kV, 40 mA, 3–99 2θ, 0.0170 2θ step for 85 s in the Department of Earth and Planetary Science at UC Berkeley.

At Pueblo Hundido (Sites 15), soil samples were collected, dried, and sieved to <2 mm. We obtained carbonate samples from site 15 and prepared them for stable isotopes and radiocarbon (^{14}C) measurements. Carbonates were obtained from coatings on clasts for ta correspondent depth. For these samples, we eliminated organic matter by washing the samples with deionized water and hydrogen peroxide (H_2O_2) multiple times. 10–100 μm of soil containing calcite were analyzed to determine $\delta^{13}C$ and $\delta^{18}O$ values using a MultiCarb system with a GV IsoPrime dual inlet mass spectrometer at the Center for Stable Isotope Biogeochemistry (CSIB) at UC Berkeley. Radiocarbon analysis was performed at the Accelerator Mass Spectrometry facility at the University of California at Irvine (UCIAMS). Radiocarbon ages were calibrated using CALIB 7.0 (curve SHCal13) and are reported as thousands of calibrated years before present (ka).

2.25 cm radius mini-disk infiltrometers (Decagon Devices) were used to measure soil hydraulic conductivity in-situ at eight locations (sites 1, 2, 7, 9, 12, 14 and 15). Infiltrometers were placed on a smooth surface spot, or where the surface was irregular, on a thin layer of sand. We recorded the volume of water that had entered the soil at regular intervals. Soil hydraulic conductivity (equivalent to steady state infiltration rates) was determined following Zhang (1997). For details see supplementary material.

4. Results and discussion

4.1. Mineralogical changes due to rain

Following the rain in 2015, desert soil surfaces had not fully collapsed and maintained high rates of infiltration, but nonetheless underwent measurable physical and chemical changes relative to pre-rainfall conditions. First, the landscape still bore a thin veneer of a salt efflorescence that had formed following the rainfall. In August 2015, the salt accumulations were more prominent and widely dispersed than in January 2016. Thus, they appear to be ephemeral accumulations, removed through a combination of wind deflation and fog reactions. The chemistry and mineralogy of a few efflorescence samples from the Oficina Rosario site (12) revealed gypsum, bassanite and thenardite. Thus, the likely mechanism for the formation of these crusts is from the penetration of the rainfall into the surface, and the upward migration – by evaporative processes - of the more soluble $NaSO_4$ salts from the largely $CaSO_4$ matrix.

Second, one of the distinguishing pre-rainfall features of the Atacama Desert was its soft and porous anhydrite layer. In many locations, it made walking, and particularly driving, difficult. Footprints and truck tires commonly sank through the material down to the underlying petrogypsic layers. Following the 2015 rain, the qualitative character of the surface in the locations we examined had undergone a profound change, being seemingly significantly hardened. We consistently noted that the land surface was more compact, less prone to dust cloud generation, and truck tracks did not sink as deeply as had done previously. Archived samples allowed us to quantify these changes. The bulk density of surficial sulfate sampled in 2016 was compared with measurements by Ewing et al. (2006) for the Yungay site (Site 7b) and Owen et al.

(2013) for the Oficina Rosario site (Site 12). Bulk density change from before (mean = 0.452 Mg m^{-3}; sd = 0.251) to after (mean = 0.598 Mg m^{-3}; sd = 0.247) the rainfall is not statistically significant at the 95% level (n = 26; alpha = 5%; p-value = 0.190), but the mean density had clearly increased. The fairly large variability is likely due to both the restricted sample size and the inherent natural spatial variability of the surface layer (See section 4.2). However, if a more relaxed statistical benchmark is used (80%), then the 32% greater bulk density of the post-rain samples statistically supports our qualitative observations.

Third, we found that the calcium sulfate mineralogy of the upper sulfate-containing layers (horizons Byk1, Byk2, Byk3 and By at Yungay) was different from that of samples collected before the rainfall (Table S3). At Oficina Rosario (OR) and Yungay (Sites 12 and 7b), XRD analyses of samples collected before the rainfall revealed only the presence of anhydrite in the uppermost horizon (Byk2), while gypsum and bassanite appeared in the same horizons in samples collected in January 2016 (Oficina Rosario) and August 2015 (Yungay). Two other sites, from which we do not have archived samples, revealed the presence of gypsum and bassanite (Oficina Americana, site 5) and anhydrite and bassanite (Barazarte, site 9) in January 2016. The presence of anhydrite in the upper 30 cm has been documented by several teams (Cosentino et al., 2015; Ewing et al., 2006; Melchiorre et al., 2018; Pueyo et al., 1998; Rech et al., 2003; Sutter et al., 2007) though the presence of the sulfate hydrate mineral basanite has been rarely reported (Finstad et al., 2018; Shen et al., 2020; Voigt et al., 2020). At normal soil surface conditions (water activities above 0.77 and temperatures around 20 °C), gypsum is thermodynamically stable with respect to anhydrite (Hardie, 1967). Anhydrite may form due to two mechanisms: (1) dehydration of gypsum at low humidity when the temperature exceeds 42 °C (James, 1992), or (2) due to direct precipitation from a highly saline solution (Freyer and Voigt, 2003). While the latter process could explain the occurrence of anhydrite at considerable soil depths (such as below 40 cm at Yungay), the widely documented occurrence of anhydrite throughout the Atacama is more likely explained by common high temperatures and low relative humidities in the soil surfaces. Nineteen months of soil climatology at Yungay (Site 7b) showed maximum temperatures of 61, 42, 36, and 29 °C at 1, 5, 10 and 20 cm depths respectively (Fig S3). The upper 10 cm of the soil were near the threshold value of the literature for gypsum dehydration. The maximum temperatures were in layers that contained pre-rainfall anhydrite (~1–12 cm) at Yungay and Oficina Rosario. Considering the long timespan of soil

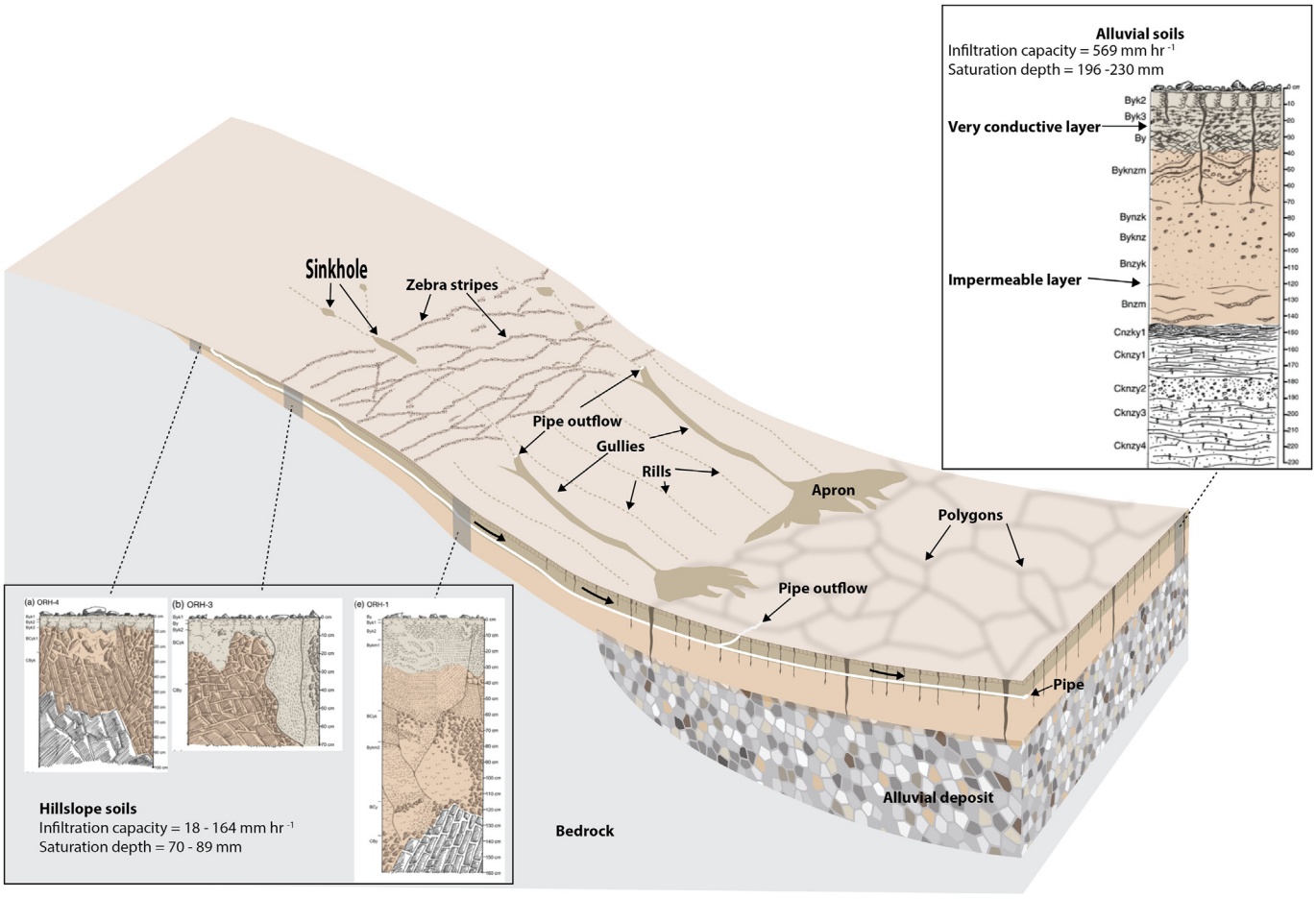

Fig. 4. Schematic figure of a typical soil toposequence in the absolute Atacama Desert. Both hillslope and alluvial soils have accumulated atmospherically deposited salts and are free of vegetation. Hillslope soils develop on weakly fragmented bedrock lacking evidence of chemical weathering and soils become thinner towards the hilltop and thicker towards the footslope. Soil in all sites have a similar sequence of horizons with a very porous and conductive layer of anhydrite on top of a cemented gypsum layer, which is mostly impermeable except for vertical cracks that penetrate up to ~1.5 m deep. Large scale polygon structures that extend to the surface occur on 1.5 to m scales. Pipes develop on top of the impermeable sulfate layer at several locations. Pipes converge with gullies on hillslopes, and pipe outflows in alluvial fans. Upper hillslopes are soil or rock mantled depending on the location. Zebra stripes commonly develop on the middle slope section, while rills occur more frequently toward the lower slope positions. Alluvial fan soil illustration is from Ewing et al. (2006) and hillslope soils illustrations from Owen et al. (2013).

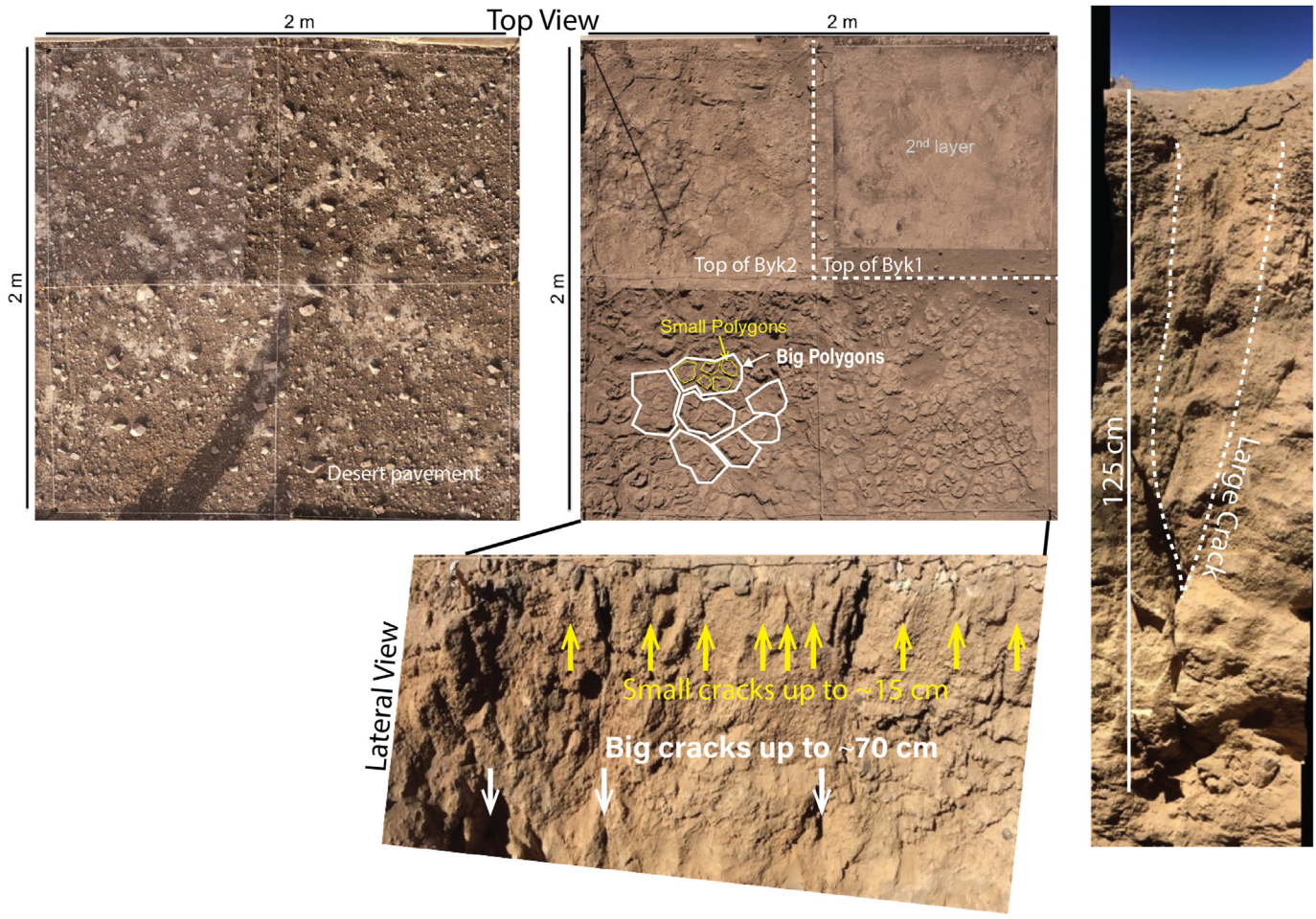

Fig. 5. Spatial distribution of sulfate polygons at the Yungay site. (a) the original surface with desert pavement, (b) desert pavement removed revealing the surface of the second layer of silt and sand (upper right square), and a third layer (bottom squares) of ~10 cm thick prisms of gypsum. These have rounded caps that are grouped in clusters separated by cracks. (c) The soil profile with cracks and polygons that form the upper sulfate layer; small cracks separate small polygons while big cracks separate big polygons (bottom image). (d) A vertical crack observed in the soil trench at Yungay, which reaches ~125 cm in depth.

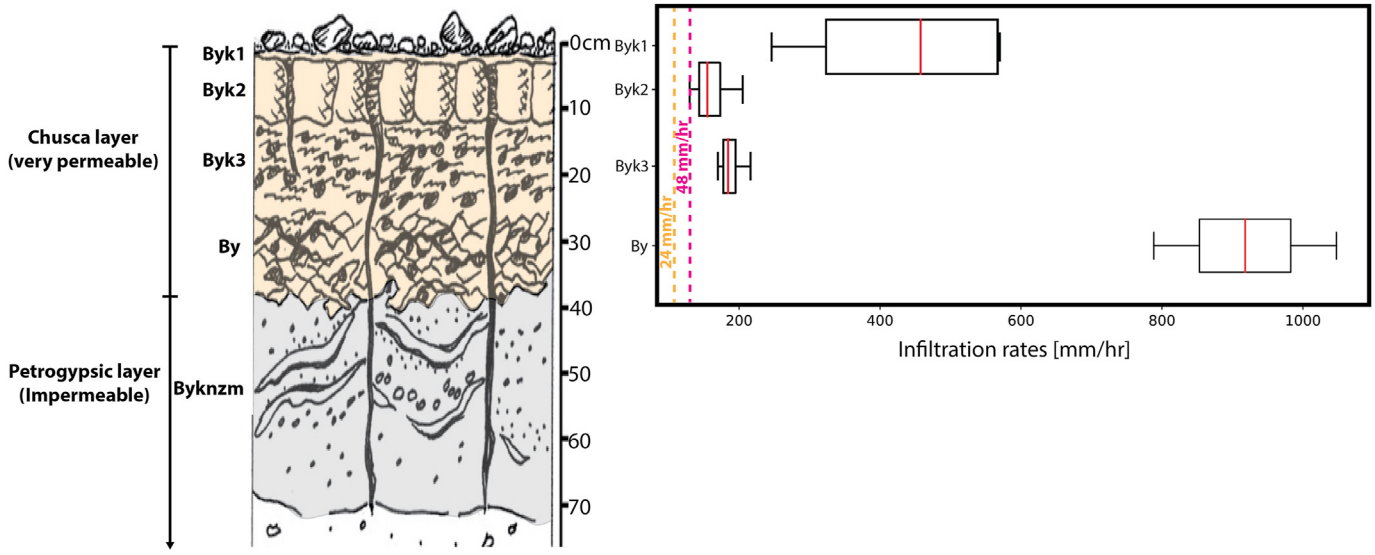

Fig. 6. Yungay profile showing infiltration rates (e.g. saturated hydraulic conductivity) measured at different soil depths. Historical rainfall rates for 1991 at Antofagasta (24 mm hr^{-1}) from Garreaud and Rutllant (1996) and for 2015 at Taltal (48 mm hr^{-1}; this work) are included for reference.

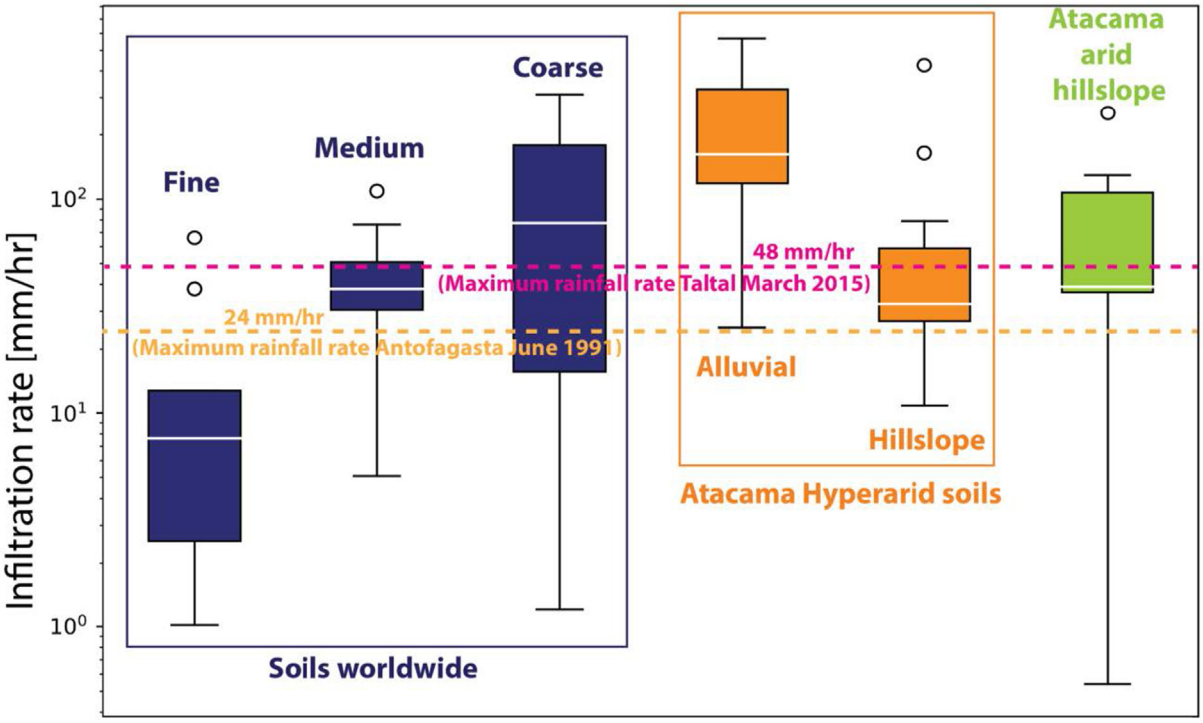

Fig. 7. Box plot with infiltration rates for soils in the Atacama desert, obtained in this study and by Owen et al. (2013), compared to infiltration rates obtained from the literature for soils of a range of textures (data obtained from Gifford and Hawkins (1978); Hillel (1982)). In the box plots, the lower boundary indicates the 25th percentile while the upper boundary the 75th percentile, the white line within the box marks the median. The circles represent outliers. Notice that y-axis is in log scale. Soil texture equivalences: Coarse = sand and loamy sand; Medium = loam, sandy loam and silty loam; Fine = clay and sandy clay.

formation in the Atacama, and the prolonged dry periods that have occurred between rainfall events (Fig S1), gypsum dehydration by low humidity and high temperatures likely maintains anhydrite. In contrast, the apparent transient presence of gypsum is due to the conversion of anhydrite to gypsum and bassanite through hydration (Freyer and Voigt, 2003), and/or through anhydrite dissolution and re-precipitation as bassanite and gypsum (Hardie, 1967; Van Driessche et al., 2012). Recent findings reported by Shen et al. (2020) at five sites affected by the 2015 march rainfall, show the presence of anhydrite and bassanite in 2012 while these minerals disappear for the same sites in 2017. They also show that chloride disappeared from the surface after the rainfall. Based on a surface sampling effort up to 40 cm in 2017 and 2019, Voigt et al. (2020) found a spatial distribution of gypsum, anhydrite, halite and nitrates that follow what they interpreted as aridity gradients, with anhydrite disappearing from surface samples toward the southern section. More likely, it seems that their observed distribution confirms the effect of the 2015 rainfall on the phase change from anhydrite to gypsum, as numerous authors (Ewing et al., 2006; Melchiorre et al., 2018; Rech et al., 2003; Shen et al., 2020; Sutter et al., 2007) observed anhydrite dominance in the same areas where, according to Voigt et al. (2020), gypsum dominates.

4.2. Desert soil architecture and infiltration

There is a continuum of surficial soil features that extends from bedrock hillslopes to deep alluvial landforms (Fig. 4). Here, we begin by discussing the alluvial sections, and then follow with a discussion of the hillslopes.

We begin with the nature of the soil and soil hydrology of a Plio-Pleistocene alluvial fan near the abandoned village of Yungay (site 7b), a site already examined (Amundson et al., 2012a; Ewing et al., 2006, 2007, 2008a, 2008b; Jungers et al., 2013). The pre-rain profile consisted of an incomplete desert pavement overlaying a ~15 cm thick layer of low density (bulk density ~ 0.7 g cm^{-3}), highly porous anhydrite polygons with eolian dust concentrated in the polygon interfaces (Fig. 5, S60). Below that, gypsum/anhydrite polygons of much higher density and width extend to a >1 m depth. Hillslope sites (sites 2, 4, 7a, 8, 9 and 12) tend to have similar features (pavement, soft porous anhydrite polygons), although the thickness and continuity of the sulfate layers is lower than on level alluvial fan surfaces.

The particular architecture of this soil is reflected in the water movement as shown by infiltration experiments. In the surface horizon, water infiltrated the soil (Horizon Byk1) downwards, and then laterally (1.5 cm) at very high rates (252–568 mm hr^{-1}). Infiltration rates into the Byk2 layer (consisting of somewhat brittle calcium sulfate rounded caps covering sulfate polygons) were lower and more consistent than at the surface (Fig. 6). The removal of the sulfate rounded cap exposed the soft and porous anhydrite layer (Byk3) underneath. Infiltration rates were slightly higher (Fig. 6), with a dominantly vertical movement. The lower section of the examined layers (horizon By) appeared to be softer and less resistant to deformation than the upper layers (Byk1, Byk2 and Byk3), and had very high infiltration rates (788–1047 mm hr^{-1}), which is rare for any soil reported in the literature (Fig. 7). The high infiltration rates in the lowest section reflect preferential flow along polygon cracks, as well as the porous, water absorbent materials.

The infiltration rates for all soils are given in Table S4. Fig. 7 summarizes the infiltration rates obtained for alluvial fans (1, 7b and 9) and steeper hillslopes (Sites 2, 12, 14 and 15) in comparison to infiltration rates reported in the literature for different soil textures. In the Atacama Desert, infiltration rates are one order of magnitude higher than for the coarse textured soil reported in the literature, with values ranging from 25.2 up to 568.8 mm hr^{-1}. On hillslopes in the desert, the rates are similar to medium textured

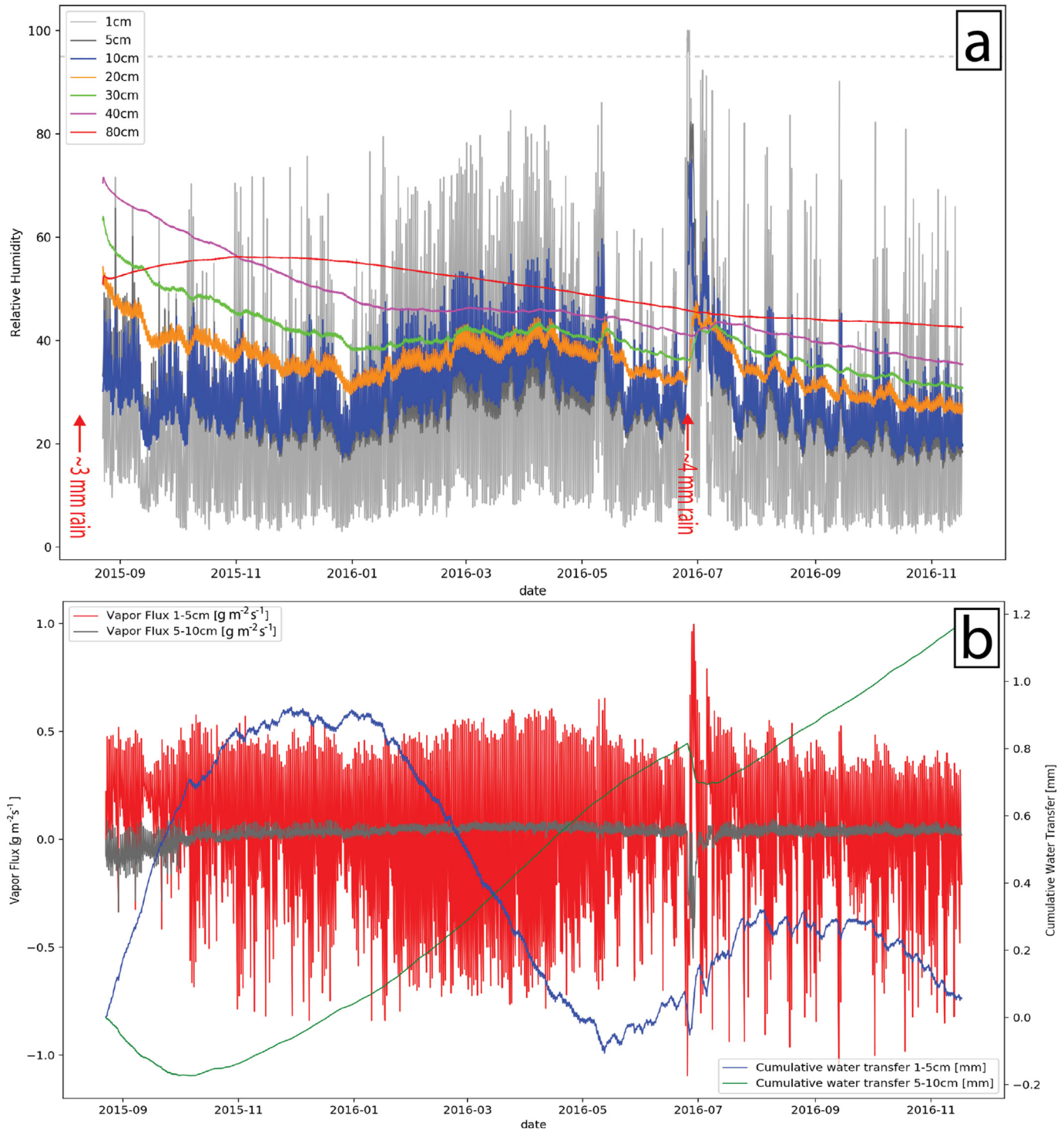

Fig. 8. Soil meteorological data collected between August-22-2015 and November-11-2016: (a) Soil RH with dashed line at 95% where liquid water is expected to exist and b) soil vapor flux vs. depth at Yungay.

soil, though a few measurements produced rapid infiltration rates (from 10.8 to 164.3 mm hr^{-1}). Most of the infiltration rates measured are much greater than the maximum rainfall rates for the storms of June 1991 and March 2015 at Antofagasta and Taltal, respectively. Only in two (sites 2 and 14) out of seven locations (Table S4) did the rainfall rates, estimated with satellite data (TRMM) approach the soil infiltration rates. Shallow lateral subsurface flow seemed to be an important feature in most of the hillslope and alluvial soils we encountered and was also observed during sprinkling experiments performed by Owen et al. (2013). Although fragile, the porous anhydrite and dust surface layers appear to have largely persisted without collapsing in most locations. The rate at which the top layer absorbs water was recently observed by May et al. (2020) to be at least 46 mm h^{-1} for a

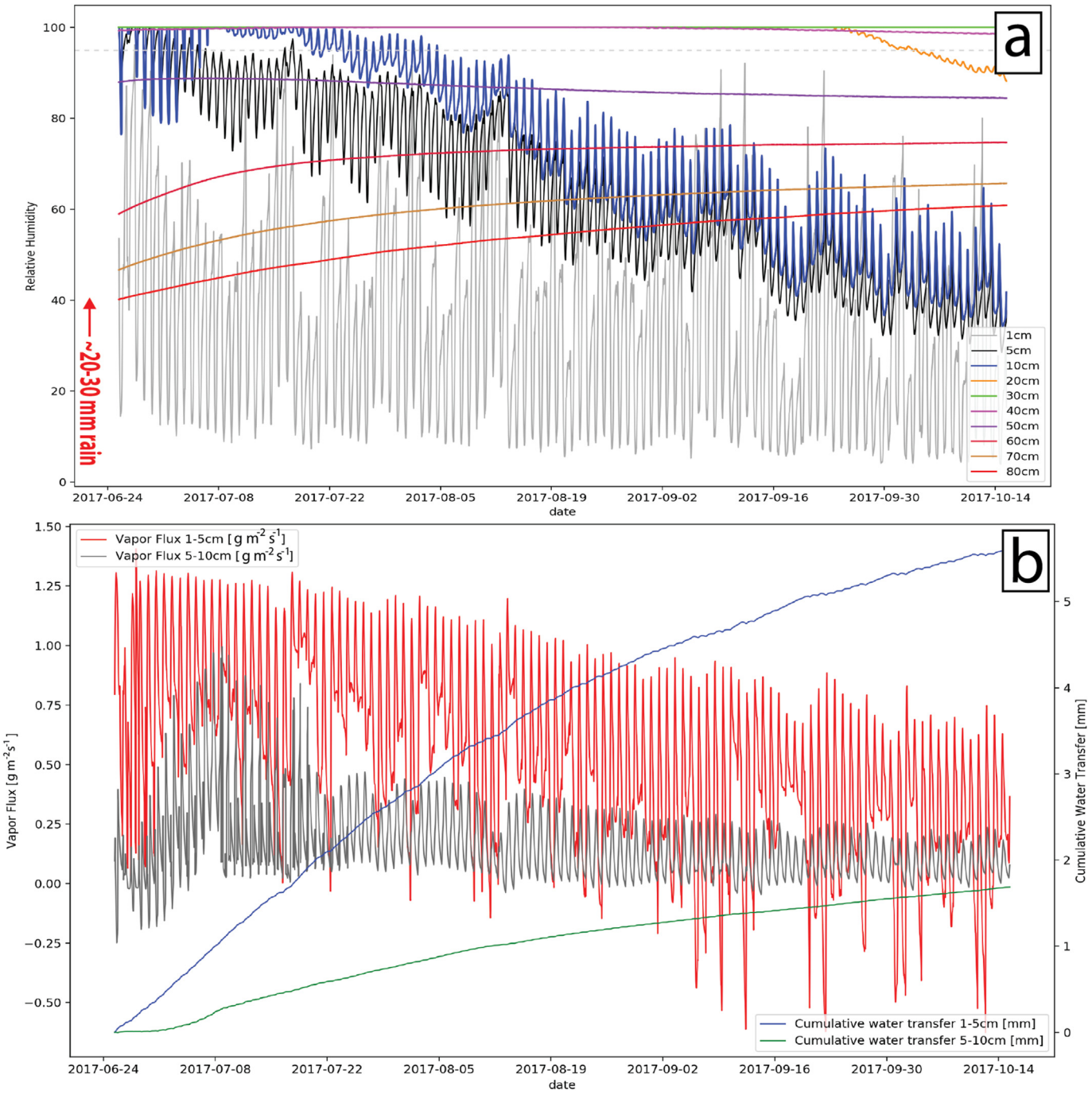

Fig. 9. Soil meteorological data collected between June 26th, 2017 and October 15th, 2017:(a) Soil RH with dashed line at 95% where liquid water is expected to exist and (b) soil vapor flux vs. soil depth at Yungay.

hillslope soil north of our study area. Our measurements show that high infiltration rates were preserved even after the rainfall, as they are similar to those measured by Owen et al. (2013).

4.3. Soil hydrological dynamics after the rainfall

Instrumentation installed in the soil on the alluvial fan near Yungay (site 7b) captured the post-rainfall soil water response from August 2015 through November 2016 (when the sensor memory was full). On June 26th, 2017, the sensors were reset to monitor soil RH and temperature after another rainfall [20–30 mm] that had occurred 20 days earlier, on June 6th, according to Jordan et al. (2019). Because the June 2017 rainfall was similar in magnitude to that of March 2015 for this site, the two data sequences provide complementary views of soil unsaturated water dynamics.

The RH data collected between August-22-2015 and November-11-2016 provides soil moisture dynamics for the 5th to the 16th month following the 2015 rain (Fig. 8a). The upper layers (1–10 cm) had very low, but diurnally dynamic, RH values with a median value of about 30% RH. RH values increased to nearly 80% at night and

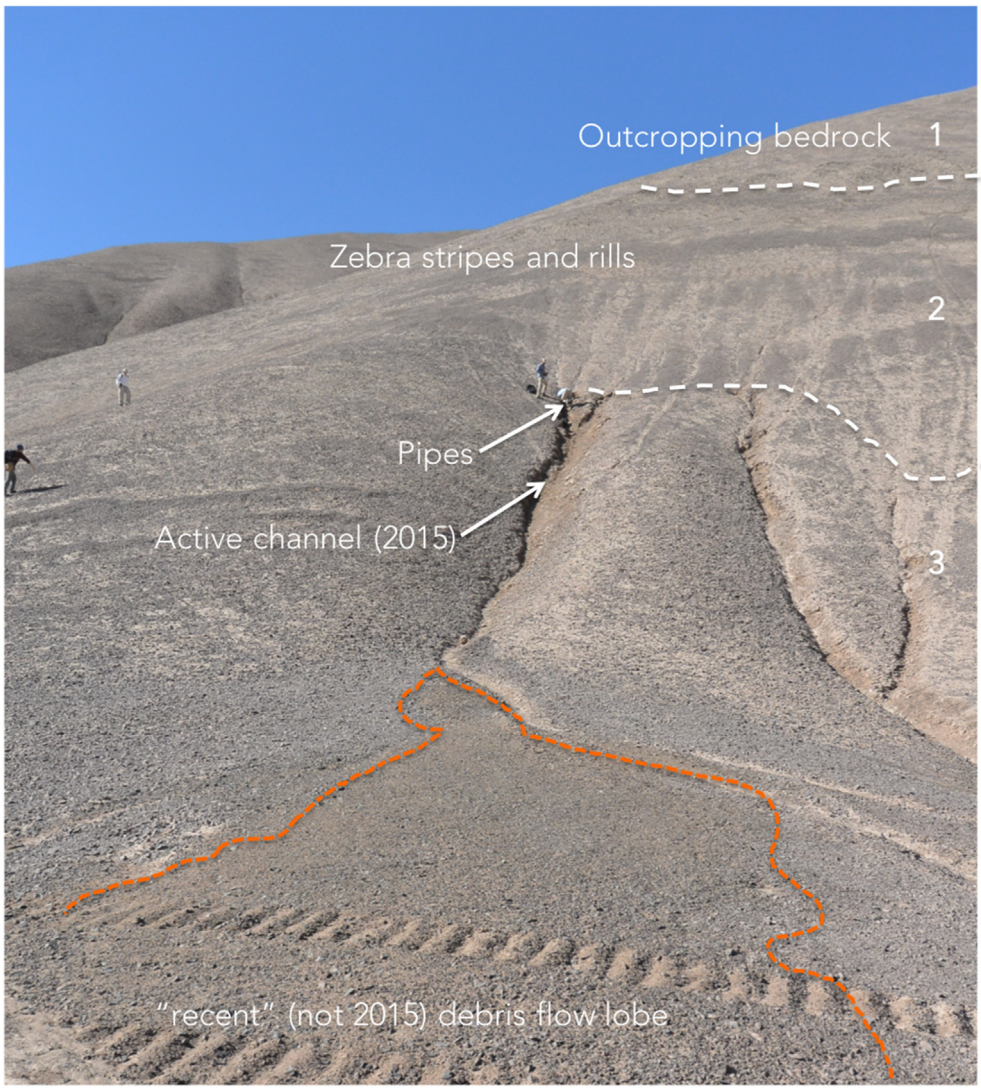

Fig. 10. Hillslope at Lomas Negras (site 4) showing three distinct zones from summit to base: 1. Upper 45 m: bedrock exposure of the metasedimentary Sierra del Tigre Formation. Some of the channels are headed by pipes. During this rain, pipes did not appear to have received any water, and the channels received their water from overland processes. The exposed material on the channel floors is composed of halite cemented sediment and saprolite.

decreased to <10% during the daytime. The diurnal effects decreased with depth and are largely muted at 30 cm. Depths between 30 and 50 cm experienced a continuous decrease in RH over time, while in the 70 cm and 80 cm depth RH increased until the 7th and 8th months respectively after the rainfall. Following this period of RH increases, these depths then experienced a drying phase.

Vapor fluxes between the 1 to 5 cm, and the 5 to 10 cm depths were estimated using Fick's law (See supplementary material). To compute water vapor flux, all dependent variables of supplemental equations 3-6 were calculated at each time step (= 30 min). Parameters for calculations are derived from measurements on a soil core at 15 cm depth-the hard bottom of the soft anhydrite layer. The Van Genuchten (1980) parameters obtained from this core and used here were $\theta_r = 0.014$; $\theta_s = 0.708$; $n = 1.66361$; $\alpha = 0.18024$. (θ_s = saturation volumetric content, θ_r = residual water content; n and α are empirical parameters). In addition, cumulative transfer through time across layers was estimated based on vapor flux computations.

There was a higher amplitude of daily variations of water flux between the upper layer 1 (1 to 5 cm) (mean = 0.0012 $gm^{-2}s^{-1}$; min = −1.0956 $gm^{-2}s^{-1}$, max = 0.9964 $gm^{-2}s^{-1}$) than between the lower layers (5 to 10 cm) (mean = 0.0269 $gm^{-2}s^{-1}$; min = −0.5508 $gm^{-2}s^{-1}$, max = 0.0986 $gm^{-2}s^{-1}$; Fig. 8b). The cumulative vapor flux shows a net transfer of vapor downwards from 5 to 10 cm between 22 August and October 05, 2015 (Fig. 8b), while after that there was a net upward transfer of water vapor. This trend was interrupted by a short hiatus of 10 days (June 24, 2016 and July 05, 2016) when rainfall of ~4 mm occurred (Jordan et al., 2019), causing a downward net flux of vapor that persisted for 18 days . The effect of this rain was propagated to depths >10 cm for a month or more after the event. The cumulative water vapor flux in the upper layer (1–5 cm) during this period showed a rapid upward flux that lasted a few weeks. The increase in RH at the layer from 1 to 5 cm following the June 2016 rain was presumably due to water vapor fluxes occurring from both directions. Fog or dew deposition are poorly documented yet might explain some of the prolonged net downward fluxes.

The RH data between June 26th, 2017 and October 15th, 2017 shows three distinct trends (Fig. 9a). First, because measurements

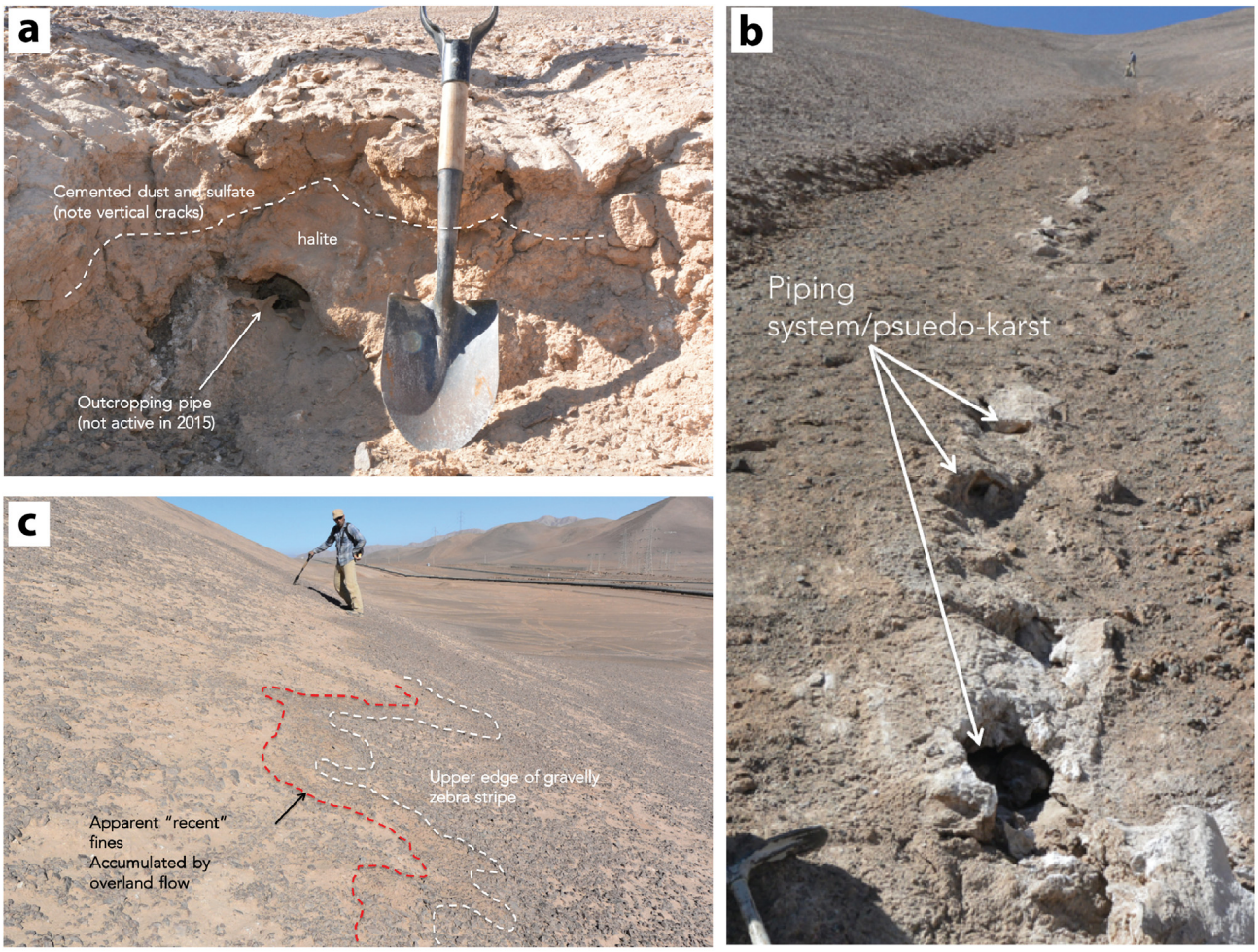

Fig. 11. Hydrological features at Lomas Negras (site 4): (a) An outcropping pipe at a knickpoint on a hillslope rill. The pipe did not carry water during the March 2015 event; (b) The pipe collapsing underneath a channel, forming pseudokarst or sinkholes structures. (c) Evidence of recent overland flow that moved and concentrated fine sediments behind a gravel "zebra stripe".

started soon after the rain, the RH of the upper depths were quite high (up to 100% at 5 and 10 cm) and decayed downward over time to about 50% or more at the end of the observation period. Second, depths between 20 cm and 40 cm had a RH > 95% for almost the entire period (111 days), a value suggested to be the threshold for liquid water by Warren-Rhodes et al. (2006). The 30 cm depth, which lies just on top of the calcium sulfate cemented layer at ~40 cm, had a static RH value of 100%, suggesting this is a hydrological barrier/perched zone. Third, from 50 cm to 80 cm, there was a smooth increase in RH with depth over time.

Upward (positive) water vapor flux rates near the surface from 5 to 1 cm were higher than at deeper depths (from 10 to 5 cm) for the entire period (Fig. 9b). Also, temporal fluctuations had a higher amplitude in the surface layers (mean = 0.52 $gm^{-2}s^{-1}$; min = −0.62 $gm^{-2}s^{-1}$, max = 1.40 $gm^{-2}s^{-1}$) than in the lower layers (mean = 0.156 $gm^{-2}s^{-1}$; min = −0,25 $gm^{-2}s^{-1}$, max = 0.99 $gm^{-2}s^{-1}$). The cumulative vapor flux was upward in the period of four months after the second rainfall, with a cumulative vapor flux of 5.62 mm and 1.68 mm for upper (5 to 1 cm) and lower (10 to 5 cm) layers, respectively. Assuming that the non-linear trend observed in the upper section continues, it could take ~480 days for the estimated 40 mm of rainfall to evaporate at the Yungay site.

The 2015 rainstorms, combined with the additional storm in 2017, appear to be relatively unusual water inputs to this soil. The dynamics of water vapor movement indicate that it may take a year or more for most of the water to evaporate. This is consistent with the results of the large InSAR transient response of land surfaces (Jordan et al. (2020).

Prior to the rainfall, the regional soil upper most layer was a soft, porous anhydrite layer. Coupled with this are mineralogical changes that must occur to return the surficial sulfates to a largely anhydrite mineralogy. We have no relevant information for speculating how, or if, the soil surface bulk density will again decline, and regain its soft and loose nature. Ewing et al. (2006) speculated that the surface salt/dust and polygons are the result of late stage (e.g. Holocene) aerosol deposition and very small wetting events, while recently Ugalde et al. (2020) proposed a Plio-Pleistocene origin for the surface layer. Thus, one hypothesis is that the surficial perturbations to the Yungay regional surfaces might require hundreds to thousands of years of time to return to their original state. However, those slight physical changes do not seem to impact water infiltration as seen in section 4.2 and therefore might also not affect the soil's susceptibility to erosion.

4.4. Water flow architecture of alluvial fans

The infiltration rate changes with soil depth as indicated in the

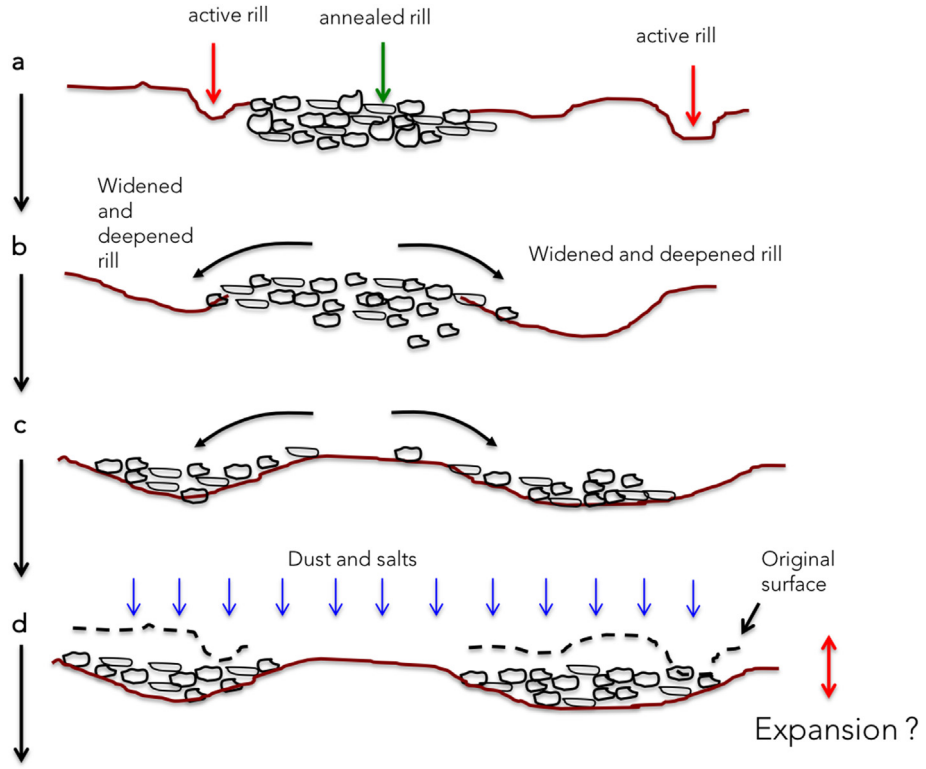

Fig. 12. A model of the sequence of processes that form and alter rills on hyperarid hillslopes in the Atacama Desert.

previous section, suggesting differences in hydrological conductivity with depth and the likelihood of lateral flow. On both hillslopes (discussed next) and alluvial fans, subsurface piping systems have developed, apparently over the dense and hard sulfate polygons that exist at 20–30 cm below the surface. On a Miocene alluvial fan east of Yungay, a highly developed piping network exists (sites 5 and 6; see Fig. 12 in Amundson et al., 2012b).

An enigmatic feature associated with these pipes is the distinctive circular depressions that dot the landscape (Fig. S61). Informally, we refer to them as "vernal pools", yet rather than being ephemeral pools, they appear to form from the upwelling of water, through "spouts" or cracks, and the spreading of this water across the land surface. These features appeared to have been activated by the 2015 rains, since recent truck tracks had been erased by upwelling and flooding. The pools are subtle depressions that have: (1) centimeter-scale depression relative to surrounding landscape, (2) thin dust accumulation over well-cemented $CaSO_4$, in contrast to a 10–15 cm thick soft calcium sulfate layer on adjacent non-stained pool in a fan surface and (3) a hole possibly corresponding to a pipe entrance observable roughly in the center of the pool. The depressions lack any contributing areas, rills or depressions that could funnel water or sediment to the depressions, and likewise lack appreciable sediment collected on the surface from flow either into or out of the central pipes. The pool depressions are characterized by a darker coloration with a 1–2 m radius. A survey of site 5 revealed roughly 35 pools per hectare, 10% having pipes easily visible from the surface.

Google Earth imagery from 2016 shows that the pools can be found on the gentle slopes between fan surfaces and incised channels. However, they are also found on top of nearly flat fan surfaces with no apparent upslope catchment. One of two models may explain these features: (1) subtle overland flow and concentration from surrounding ~ 1 m higher topography, or (2) outflow from a subterranean piping system, driven by a sufficient hydraulic head. Both models suffer from a lack of empirical support. We could not identify any sign of flow from the surrounding landscape. Model 2 is supported by the fact that pools inundate features caused by human disturbance. However, the exceedingly gentle slopes of the undulating landscape make the source area and pressure sources difficult to identify. It is important to note, however, that this alluvial fan system – in outcrops observed along stream escarpments – has significant moisture in some of its basal fine-grained facies, and there seems to be water flow from upslope in the catchment, which extends high into the Domeyko Range to the east (Gamboa et al., 2019).

4.5. Hillslope soils and processes

The hillslopes within the region are mantled with ~50–100 cm of dust and salts. Thus, these geomorphic surfaces are net accretionary surfaces, but net erosional surfaces (Amundson et al., 2012b; Owen et al., 2011). However, these soils also show evidence of a variety of surficial features caused by flowing water, which we assessed for evidence of recent activation.

To begin, we consider observations made at Site 4, Lomas Negras (Fig. 10, compare also to Fig. 4). Beginning at the slope summit, along a 45 m downslope transect, the surface consists largely of exposed bedrock in the first segment, with no evidence of channelized flow. For the next 22 m, the slope is mantled with a thin soil layer (~30–70 cm of dust and salts), and with distinctive segregated rills and "zebra stripes" (Owen et al., 2013). Following this segment, the small rills irregularly coalesce into a few, distinct channels (Fig. 10), the heads (Fig. 11a) and floors (Fig. 11b) of which feature outcropping "pipes". The channels in some locations showed evidence of very minor water flow during the 2015 rain events, and the accumulation of dust within the pipes indicated that they did

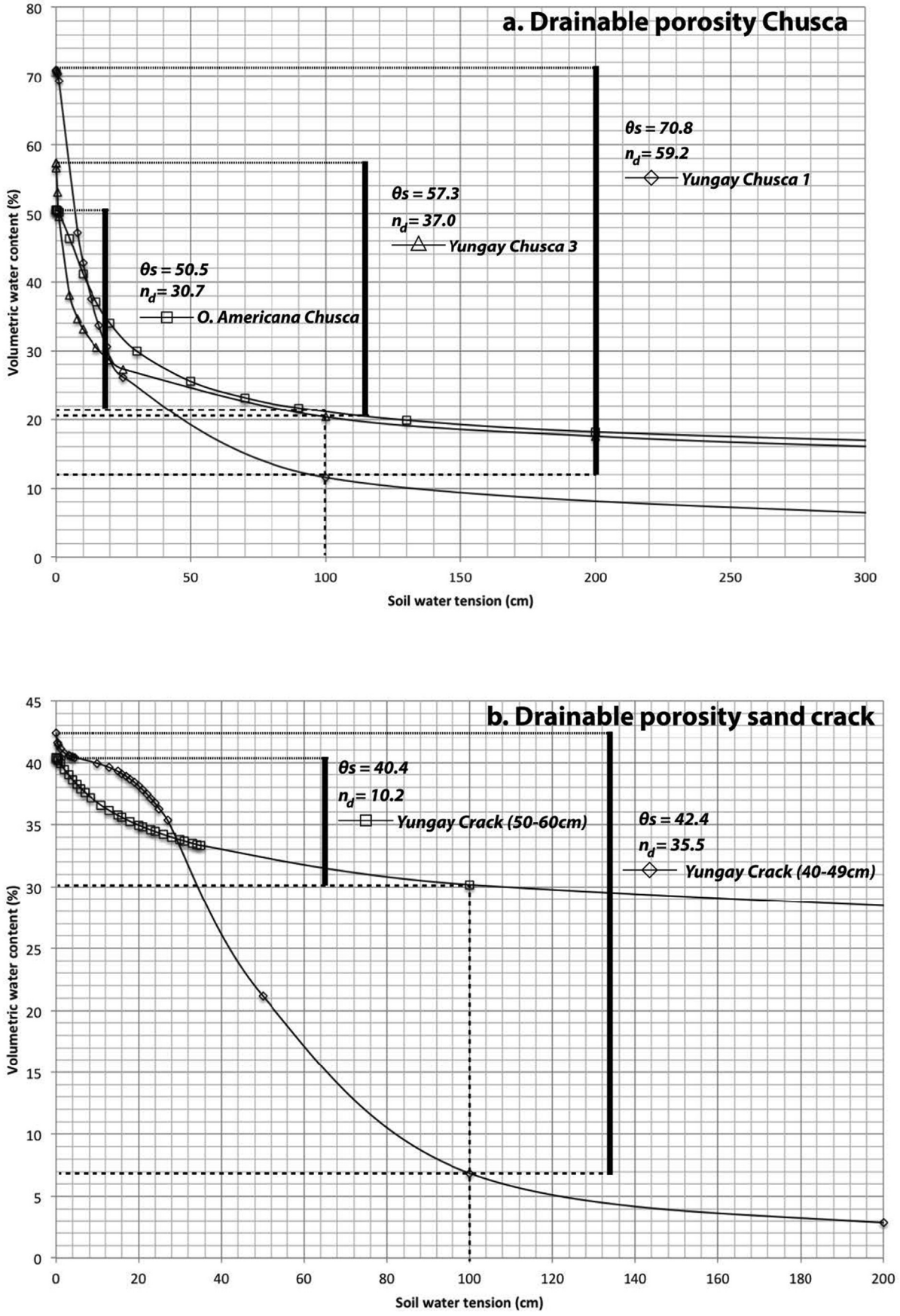

Fig. 13. Water retention curves for: (a) three anhydrite rich samples from the Atacama Desert, showing the total (θ_s) and drainable porosity (n_d) in %; (b) sand in sulfate cracks at two depths in Yungay alluvial soil (Site 7b).

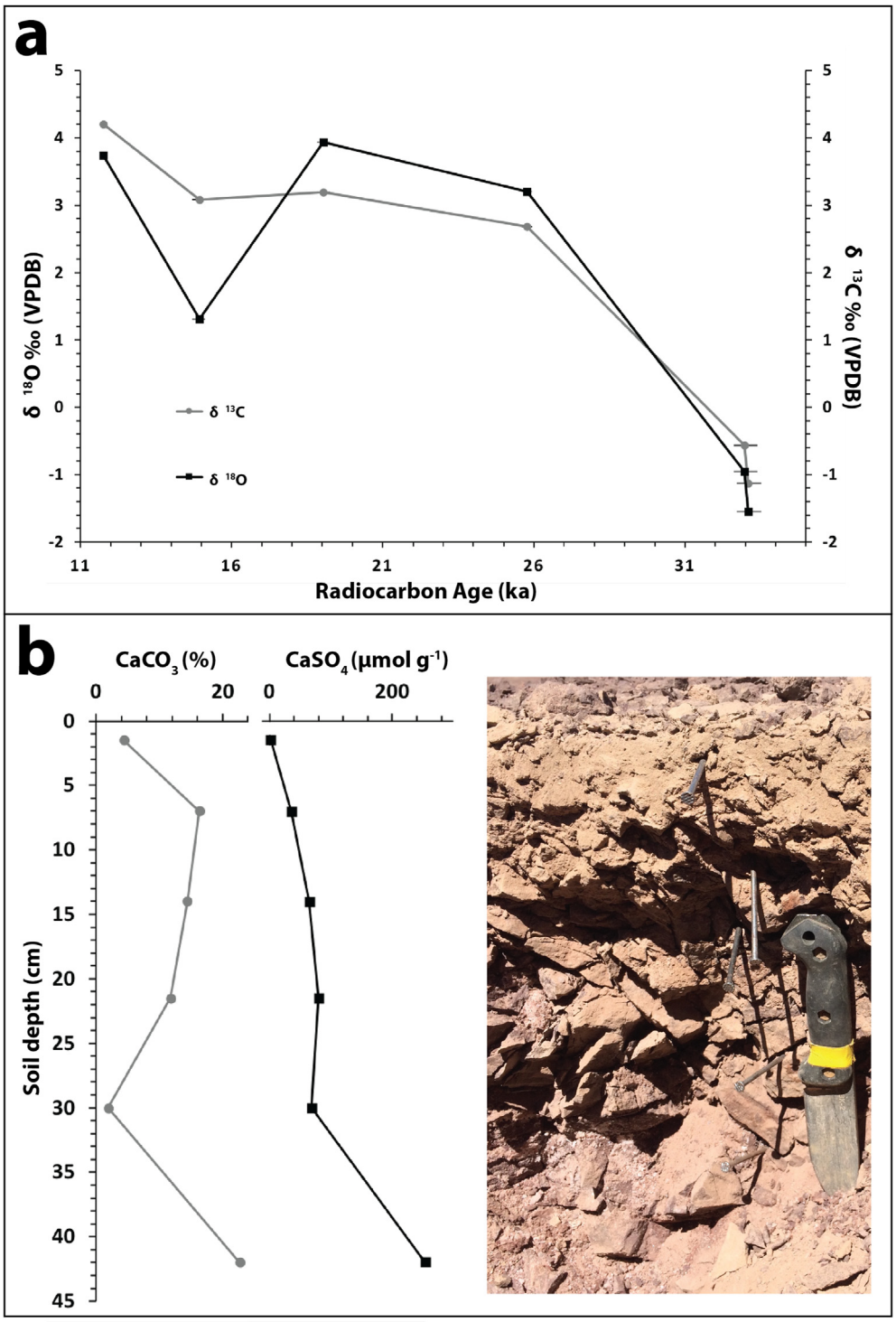

Fig. 14. Pueblo Hundido soil data (site 15). a) Measured soil $CaCO_3$ ^{13}C (‰ VPDB) and ^{18}O (‰ VPDB) values vs. radiocarbon ages of carbonate. b) Depth profiles of carbonate and sulfate concentrations, with a photo of the soil profile at the same scale. Nails mark boundaries between horizons.

not transport significant water flow during the 2015 rainfall. In some areas of the mid-section of the hillslope (rills and zebra stripes, Fig. 11c), there had been overland flow on the crusted, gravel-poor portions of the slope that in turn had mobilized and concentrated fine particles in the upper edge of the gravelly-stripes (Fig. 11c). We found no evidence that the gravel itself had moved. While the 2015 storm did not generate significant mud flows or alluvial deposits, there is evidence of morphologically 'recent', but not from 2015, lobes of mud that have accumulated at the base of the slopes (Fig. 10).

These observations suggest that rilling is facilitated by bedrock underlain hillslope areas that are capable of generating overland flow (e.g. Fig. 10). An additional mechanism by which the rills and channels develop may be through subsurface piping. We observed

pipes at sites 1, 3, 4, 5, 6, 7 and 8, and they have been previously reported by Amundson et al. (2012b) at other locations. Pipes were found at the base of a permeable soil material (gypsic horizon) which overlays halite or highly cemented sulfate (Fig. 11a). Water flow in the pipes appears to require near-saturated conditions of the overlaying material. Given that the channels have pipes at their head (Fig. 10) and have semi-collapsed pipes as their beds (Fig. 11b), it is also possible that the subsurface piping and its collapse drives rilling and the creation of channels. Similar patterns were observed with pipes in alluvial fans at La Negra (site 3), Pedro de Valdivia (site 1; Fig. S53, S54) and Oficina Yugoslavia (site 6; Fig. S55–S57). Those large pipes also showed no evidence of recent water flow (e.g. Fig. 11 a, b).

Slopes at Laguna Seca, Paranal and Pampa Remiendos (sites 8, 10 and 11 respectively) revealed more about the fluvial processes that appear to sculpt hillslope soil over long timescales. These areas appeared to have been impacted by the rainfall of March 2015 as evidenced by recent debris and mud flow. Differences in soil cover between these sites appears to be fundamental in the response to the rainfall event. At these locations, the local bedrock (volcanic and intrusive rocks) produces angular gravel that provides a discontinuous cover over the thinly soil-mantled slopes. Soil is weakly developed, with an indurated gypsum crust on top of bedrock or colluvium. At Paranal and Pampa Remiendos, rilling and mudflows occurred following the March 2015 storm, allowing us to examine mechanisms of rilling at sites with different soil covers. Debris flows at sites 10 and 11 were in close proximity, to small catchment areas (~0.75 km^2) (Fig. S36– S39). Using a range of curvature radii from 6 to 20m, k values from 1 to 3m, and a measured difference in inner and outer curve levee height of 10 cm, we estimate discharges of 0.97–2.44 m s^{-3} (more details in Supplementary materials). These debris flows occurred on slopes ranging from 10.5 to 21.5°, with sediment discharge at terminal lobes (Fig. S37) and evenly distributed along levees. Different degrees of incision occurred on different slope sections, with both steeply incised channels (Fig. S34) and deposition of sediments (Fig. S39).

Upon close inspection, most hillslope surfaces contained a complex history of surface water alteration and subsequent smoothing under dry conditions. We observed hillslope rills and channels in varying stages of formation, decay, and repair (Fig. S62). Based on these common features, we propose a model for the observed hillslope fluvial features. Fig. 12 shows a schematic representation of our hypothesis of major steps in hillslope processes. Waterflow down slopes largely appears to concentrate on gravel-poor areas (or the water may be capable of moving gravel into adjacent levees), and thus rills and small channels tend to be found adjacent to irregular stripes of gravel that are oriented perpendicular to slope contours (Fig. 12a). Over time, channel cutting proceeds and widens, under-cutting gravel-mantled slope-parallel stripes (Fig. 12b). Once this occurs, gravel is dislodged and moved by gravity into the adjacent, lower elevation channels. Eventually, this proceeds to the point that all gravel has been captured by adjoining channels, and the former gravel-covered strip now serves to form new rills. This sequence of steps constitutes a net wearing down of the landscape. However, this wearing down is partially (or fully over geological time) offset by dust and aerosol salt additions which re-inflate the landscape. In particular, the gravel is an effective dust collector, and helps to facilitate an annealing of the landscape and the partial replacement of eroded soil material. The apparent slow, but net downward, wearing of these surfaces is consistent with the region's exceedingly low rock erosion and soil production rates (Owen et al., 2011). The erosion rate at high elevation Paranal and Pampa Remiendos is likely higher than at the lower elevation at Oficina Rosario with erosion rates inferred from cosmogenic nuclide to be ~1 m/My, but with less than 10 m/My reported for Chañaral by the same authors (Owen et al., 2011), a more humid location at the southern limit of the Atacama Desert. Unlike most regions on Earth, the erosional process is a slow and erratic balance between rare fluvial processes and the persistent slow deposition of dust and salt on the landscape.

At Laguna Seca (site 8), we found many rills and channels that are fully 'annealed' and covered with dust and salts. Most of the rills with the greatest evidence of March 2015 activity occupy the linear to convex portions of the hillslopes. The depth of incision at most of the observed locations is modest (<10 cm; Fig. S63) and the maximum depth is limited by the presence of an impermeable petrogypsic horizon. Most of the channeled runoff occurred through parallel rills lacking obvious dendritic structure. However, at a larger spatial scale, the hillslopes produce a dendritic system with a low drainage density and a dendritic organization. The overall landscape seemed to be a relict feature of a period before the establishment of the current aridity. The parallel nature of rills may not be solely due to the steepest descent path of the broad paleocontours of the landscape, but may also be controlled by the permeability of the soil coverage, which might create a transient (post-storm) water table that controls the lateral spacing of the rills (Shen et al., 2015).

4.6. Rainfall thresholds for fluvial activation

A striking finding of this work is that there are abundant landscape features that reflect past surface water movement, yet few of these were activated by the 2015 rainfall. However, in many locations, we observed indications of shallow subsurface flow controlled by the soil architecture (as described in section 4.2), where a highly conductive soil layer lies on top of an impermeable layer (Petrogypsic horizon). To estimate the amount of rainfall needed to generate shallow subsurface flow, we consider a transient perched water flow at the interface between the surficial sulfate and underlying petrogypsic horizon (McDonnell, 1990). We assume that the water corresponds to water flowing through the macropores, whose volumetric quantity is represented by the drainable porosity (n_d). As shown by the soil moisture data, water transfer toward the impermeable layer (<40 cm at Yungay) is very slow even on relatively level landscapes during the recent rains. We calculated values of n_d for the highly conductive layer ($n_d = \theta_s - \theta_{fc}$, θ_s being equal to soil porosity and θ_{fc} to field capacity), using a conservative field capacity value that is equal to 100 cm of soil water tension (Weiler and McDonnell, 2004). We considered two locations, Yungay hills and Oficina Rosario (sites 7a and 12), representing two extremes in the regional erosion rates previously described by Owen et al. (2011; 2013). The thickness of the surficial sulfate layer averages 5 cm at Yungay and 14 cm at Oficina Rosario. As soil in the Atacama Desert is not expected to have received significant rainfall for decades, we considered the amount of antecedent moisture to be negligible. This means that soil pores in the unsaturated zone must be filled up to field capacity before water can rapidly move through the soil (>100 cm of soil water tension). Considering soil depths at both sites, and measured values of n_d and θ_s (Fig. 13), the amount of accumulated rain to initiate shallow subsurface flow ranges from between 5.8 and 10.15 mm for Yungay and 16.24 and 28.42 mm at Oficina Rosario. In order to saturate the conductive layer, rainfall must exceed at least 25–35 mm for Yungay and 71–99 mm for Oficina Rosario. These amounts are conservative, considering that the high conductivity of the surficial layer would require an additional infiltration flow to maintain downslope drainage and because cracks in any soil layer will transport an additional amount of rainwater to lower levels.

However, cracks also exhibit a rapid decline with depth in the number of cracks, which explains the common shallow subsurface storm flow (Weiler et al., 2005). Estimates of rainfall amounts during the March 2015 storm are above the threshold to create shallow subsurface water flow at the interface ($>\theta_{fc}$) in Oficina Rosario and are apparently able to create saturation at shallow soil depths in Yungay. Our field observations show that runoff occurred at both locations, particularly at Yungay, where numerous rills and channels may have been activated by transient soil saturation.

There are two mechanisms through which overland flow can occur in a rainstorm: infiltration-excess overland flow and saturation-excess overland flow (Smith and Goodrich, 2006). Infiltration excess occurs when rainfall rates exceed the infiltration capacity (steady state infiltration of soils) and is a common mechanism of overland flow in arid and hyperarid areas because these areas usually have very thin soil or have exposed bedrock with low infiltration capacity (Bahat et al., 2009; Cools et al., 2012; Greenbaum et al., 2006; Wheater, 2002; Yair and Lavee, 1985). Unlike most other arid regions, the soil in the Atacama absolute desert is highly permeable (See section 4.2). To trigger infiltration excess overland flow, rainfall rates must overcome average infiltration rates of 78 mm h^{-1} and 244 mm h^{-1} for hillslope and alluvial soil, respectively. While local (or depth specific) infiltration rate values can be as low as 10.8 mm h^{-1} and 25.2 mm h^{-1} for hillslope and alluvial soil, respectively (Table S4), field evidence and the high infiltration rates measured suggest that there is rarely sufficient rainfall to provoke infiltration excess in the Atacama, as was previously suggested by Owen et al. (2013) and recently by May et al. (2020). The second mechanism, saturation-excess, occurs when the soil is saturated or filled with water from a subsoil restriction, such as a shallow bedrock or a restrictive soil layer. This is generally considered to be more common in humid areas, where prolonged storms are frequent and antecedent soil moisture is significant (Smith and Goodrich, 2006). Although it is difficult to estimate the occurrence of saturation-excess overland flow in the Atacama, the occurrence of this mechanism is highly unusual if we consider that rainfall rates must maintain high rates of downslope flow due to the high conductivity of the soil. The amount of water required to create such overland flow, ranging between 25 and 99 mm of rain for hillslopes (in order to saturate the conductive layer), is about one order of magnitude greater than current annual rainfall averages for the area (Fig. 1). However, the formation and activation of pipes is an indication that, at some point in geological time, those thresholds in rainfall magnitudes were exceeded.

In summary, the fans and the variety of the hillslopes that surround them are presently buffered by a porous salt-rich soil surface that has high infiltration rates and water holding capacity. Thus, the threshold required to activate many of the semi-fossilized fluvial features that are evident is much higher than the 2015 rainfall for most of the locations observed. When rainfall capable of exceeding these thresholds last occurred is unknown. In the next section, we provide some evidence for when the last major changes in climate may have regionally occurred.

4.7. Observations and insight from the desert periphery

The southern-most extent of our observations was at the southern edge of the absolute desert near the village of Diego de Almagro, at 26.3° S (Pueblo Hundido, site 15). There, we examined a convex hillslope in a hyperarid/arid location, which was almost completely devoid of plant life. The hillslope was undergoing active zebra stripe development and had evidence of both fine particle and some coarse particle movement during the recent rains, as well as water movement through rills (Fig S25 – S27). The summit of the hill had an interlocking gravel pavement with a thin dust-rich V horizon. There was no evidence of weathering of bedrock and the most evident pedogenic processes were distinctive accumulations of both gypsum and carbonate.

The presence of significant amounts of both carbonate and gypsum together, is not typical in the absolute desert itself. In hyperarid, abiotic conditions, Ca is sequestered into gypsum or anhydrite due to an abundance of SO_4, and the very low (atmospheric) levels of CO_2 in the soils (Ewing et al., 2006; Quade et al., 2007). In the field, we hypothesized that the carbonate was a paleo-feature and might provide insight into the onset of the present hyperarid conditions, and evidence of past climate conditions. Thus, we examined the stable isotope composition, as well as the radiocarbon age of the carbonate with depth (Table S8).

An important result of the measurements is that the ages of the carbonates decrease systematically towards the surface, with the oldest radiocarbon ages being nearly 34ka, and the youngest being 11ka (Fig. 14). The simplest interpretation of the depth trend, one also observed in the Mojave Desert (Wang et al., 1996), is that the depth of water percolation steadily declined over time, decreasing the depth of the carbonate formation zone, with a termination of carbonate accumulation at the end of the Pleistocene, suggesting increasing aridity towards the Holocene.

The Pueblo Hundido site (site 15; 26.3°S) at an elevation of 1098 m lies at the summit position in a hillslope, deeply within the winter precipitation zone of the Atacama, associated with the southern westerlies. The ages obtained may thus be related to wetter periods that occurred with slight northward shifts of the westerlies (Stuut and Lamy, 2004), this is the mechanism suggested for the observed biotic record in rodent midden pollen deposits at the nearby Quebrada del Chaco (25.5°S) for sites above 2600 m (Maldonado et al., 2005). It is probable that this protracted episode of enhanced precipitation impacted sites in the absolute desert and further north, possibly activating the numerous hydrologic features that require significantly more precipitation than occurred during the March 2015 storm. Those storms may have created the zebra stripes, the rills and pipes, as well as redistributing salts and sediments locally, but were not large or intense enough to entirely remove or destroy the soils that mantled the hillslopes or remove the large quantities of salt embedded in the soils.

The stable C and O isotope composition of the carbonate coatings on the gravels show that the carbonate formed in a very arid, but significantly more vegetated, environment than today. Assuming a ~14‰ offset between soil CO_2 and carbonate $\delta^{13}C$ values (Cerling, 1984), the carbonate in the deepest and oldest soil layer formed in equilibrium with CO_2 ranging from −10 to −16‰, which are values associated with the influence of plants and microbial activity (Cerling and Quade, 1993), while higher values toward the top reflect $\delta^{13}C$ values reported by Quade et al. (2007) for near abiotic environments in the Atacama (Fig. 14). While the trend of decreasing $\delta^{13}C$ values with depth is typical for CO_2 diffusion profiles, the radiocarbon ages indicate that they formed at different times, and thus the depth trend might be best interpreted as a time sequence (Table S8). Given no evidence for any significant biological CO_2 production today, the carbonates suggest that a discontinuous and modestly productive plant cover existed when the carbonate accumulated. Even the later forming carbonate at ~11ka formed from soil CO_2 with a $\delta^{13}C$ value of −9.5‰ – much more negative than that of the essentially abiotic conditions that exist today. Assuming that past vegetation was C_3 dominated, the profile suggests a past soil respiration rate of approximately 15 g C m^{-2} y^{-1} (see Fig. 7a in Ebeling et al., 2016).

The $\delta^{18}O$ values of the carbonate also decrease with depth, from a high of 3.94‰ (VPDB) near the surface, to −1.44‰ (VPDB) found at depths similar to values and depth trends found in much more calcic and biotic soils 200 km to the S near Vallenar (Ebeling et al.,

2016). However, the samples here appear to represent a declining depth of calcium carbonate accumulation over time. The oxygen isotope composition of soil carbonate reflects the O isotope composition of the rainfall plus any evaporative enrichment. After accounting for fractionation between liquid water and carbonates of 29.1‰ at 20 °C (Kim and O'Neil, 1997) and correcting for $\delta^{18}O$ VSMOW against VPDB (Coplen et al., 1983), based on the recent $\delta^{18}O$ values for precipitation in the Atacama by Jordan et al. (2019), where Pacific sourced rainfall in the Atacama tends to be significantly higher ($\delta^{18}O$ −2 to −8‰ VSMOW) than Atlantic sources ($\delta^{18}O$ −8 to −15‰ VSMOW) it is most probable that rainfall was predominantly Pacific in origin. However, given that the youngest samples accumulated nearest to the surface, it is difficult to deconvolve the effect of changing rainfall source values from changing degree of evaporation over time, as high enrichment of $\delta^{18}O$ due to evaporation has being reported for Atacama desert soils by Finstad et al. (2016).

However considering the trend of younger carbonates toward the surface (Table S8) and that the depth of pedogenic carbonates is directly related with mean annual precipitation as reported for arid environments (Oerter and Amundson, 2016; Retallack, 2005; Royer, 1999), the carbonates suggest a progressive decline in soil moisture and depth of leaching, from 34ka to 11ka. It is probable that since ~11 ka, sulfate accumulation became the dominant sink for Ca and carbonate precipitation ceased, indicating an increase in the intensity of aridity (Fig. 14). The timing of this apparent decline in rainfall is consistent with regional trends in rainfall (Fig. 14), in particular, the cessation of wetlands or shallow lakes around the vicinity of Yungay about 10–11ka ago (Pfeiffer et al., 2018) is completely consistent with the apparent decline in soil moisture found in this soil.

If the last major climate change was more than 10 ka old, are some or many of the features described in this study fossil Pleistocene features? Most likely any of these Pleistocene fluvial features that partially remain have been modified by both dust and salt accumulation, and occasional Holocene rainfall alteration, leaving a chronological record that is complex and difficult to deconvolve.

4.8. Implications for past and future rainfall events

An expectation for greater rainfall in an entirely unvegetated landscape is that significant surface runoff will result, along with sediment and debris flows. Yet, as recently mentioned by Jordan et al. (2015, 2020), the most striking observation of the Atacama Desert following the recent "hundred-year storm" is how subtle the changes to the terrain were. The surficial anhydrite and dust underwent hardening and compaction. Some streams and tributaries were activated. Minor debris flows and rilling occurred. Yet, these processes were not uniform, and responded quite differently to local variations in soils, as well as to orographic effects.

Somewhat unexpectedly, we now hypothesize that the lifeless Atacama Desert exhibits a significant degree of hydrological resilience to rainfall. This is not a resilience arising from biotic-abiotic feedback controlling Earth surface processes (Corenblit et al., 2011), but rather from the enormous quantities of salt and dust that have mantled this region since at least the late Pliocene times (Amundson et al., 2012b). The term "resilience" implies both the presence of a threshold, and the ability to "bounce back" after a perturbation if the threshold is not exceeded. We have been able to place at least first order constraints on the thresholds required to initiate more significant, if not catastrophic, landscape responses to rain. Overland flow by saturation-excess is unlikely under current conditions, requiring approximately 30 mm of rain at Yungay and 70 mm for Oficina Rosario. This is a lower limit of rainfall needed to activate the now semi-fossilized fluvial features that are common in the region.

The evidence compiled in this work suggests that a "century scale" rainfall, like the one that occurred in March 2015, is not large enough to activate many of the numerous erosion mechanisms that have left their mark on the absolute desert (Table S14 and S2). The rainfall thresholds necessary to create runoff and erosion in the absolute desert seem to be at least one order of magnitude higher than that of the March of 2015 rainfall for most locations observed (see section 4.7). Soil geochemistry evidence provided here suggests that the late Pleistocene may have been more conducive to causing these features to be more frequently active. Yet, these pluvial episodes were not so extreme or protracted as to remove the bulk of the salts from the alluvial and hillslope surfaces in the region. Throughout its long history, it seems that the Atacama Desert has occasionally teetered near a rainfall threshold that, if larger or longer, would have changed much of what makes this such a unique environment.

Yet this remains a delicate threshold. Changes in global climate and oceanic patterns have been suggested to potentially increase moisture in the region (Urrutia and Vuille, 2009). Once the region's soil-mediated threshold is surpassed, it would seem that the landscape response could be catastrophic.

Increased development of infrastructure in the region (e.g. huge solar power plants, roads, pipes and mining operations) should consider the future environmental factors and the possible impacts on their operations. None of the Desert's internal drainage has a hydrometer to measure surface water flow. The large hydrological variability of arid areas requires this investment. Wheater (2002) emphasized the difficulties in deriving reliable long-term hydrological records in arid regions. In a region with so much sediment poised to respond to a climatological threshold, understanding changing climatic patterns and their potential impacts is critical for economic and humanitarian reasons.

5. Conclusions

The evidence compiled here suggests that the soil has an important influence on the landscape's response to rainfall in the Atacama Desert. While rilling and overland flow occurred in areas at the southern border of the absolute desert and in the Coastal Range during the March 2015 storm, the driest section of the desert covered with salt-rich soils possesses physical properties that allow the landscape to resist the impact of rainfall on erosion. Most of the changes that affected the desert were ephemeral changes in soil, such as soil profile wetting and redistribution of salts. Unlike some arid and hyperarid areas in the world that are susceptible to high intensity rainfalls, the absolute desert of the Atacama resisted the force of a "century scale" rainfall, like that which occurred in March 2015.

It is evident that larger rainfalls occurred in the region at some point in the past and, near the southern limit of the absolute desert, radiocarbon and stable isotope evidence from soil carbonate suggests a declining rainfall regime, with biotic conditions, from 30 ka to 11 ka, at which time carbonate formation ceased and most vegetation disappeared. Thus, it is plausible that some of the visual evidence of fluvial moderation of landforms and soils is a relict feature of Pleistocene conditions.

The landscape of the present absolute Atacama Desert has a resilience to impact from rainfall due to the incredibly high rates of water infiltration into anhydrite rich soil. The apparent threshold for significant alteration of the landscape may require a total rainfall of about an order of magnitude larger than those recorded in the past several hundred years. The threshold values for a single rainfall event to initiate shallow subsurface flow are approximately

5.8–10.15 mm for alluvial fans and 16–28 mm for hillslopes. In order to initiate overland flow due to saturation-excess rainfall must exceed 25–35 mm for alluvial fans and 71–99 mm for hillslopes. The rainfall rates required to produce infiltration-excess overland flow must exceed 78 mm h^{-1} for hillslopes and 244 mm h^{-1} for alluvial soils.

Yet these amounts are small in an absolute sense and underscore the unique set of conditions that maintain this most unusual environment on Earth.

Author contributions

M.P. A.H. and R.A. designed research; M.P. A.M., A.H., T.J., A.H., and R.A. performed research and analyzed data. M.P., and R.A. wrote the paper. All authors checked and agreed to this version of the manuscript.

Declaration of competing interest

The authors declare that they have no known competing financial interests or personal relationships that could have appeared to influence the work reported in this paper.

Acknowledgments

Funding was provided by through the CONICYT Becas Chile Scholarship and the Fulbright Foreign Student Program Scholarship (M.P.) and through NSF RAPID GRANT (R.A.).

Appendix A. Supplementary data

Supplementary data to this article can be found online at https://doi.org/10.1016/j.quascirev.2021.106797.

References

Amundson, R., Barnes, J.D., Ewing, S., Heimsath, A., Chong, G., 2012a. The stable isotope composition of halite and sulfate of hyperarid soils and its relation to aqueous transport. Geochem. Cosmochim. Acta 99, 271–286.
Amundson, R., Dietrich, W., Bellugi, D., Ewing, S., Nishiizumi, K., Chong, G., Owen, J., Finkel, R., Heimsath, A., Stewart, B., 2012b. Geomorphologic evidence for the late Pliocene onset of hyperaridity in the Atacama Desert. Geol. Soc. Am. Bull. 124 (7–8), 1048–1070.
Bahat, Y., Grodek, T., Lekach, J., Morin, E., 2009. Rainfall–runoff modeling in a small hyper-arid catchment. J. Hydrol. 373 (1), 204–217.
Barrett, B.S., Campos, D.A., Veloso, J.V., Rondanelli, R., 2016. Extreme temperature and precipitation events in March 2015 in central and northern Chile. J. Geophys. Res.: Atmosphere 121 (9), 4563–4580.
Betancourt, J., Latorre, C., Rech, J., Quade, J., Rylander, K., 2000. A 22,000-year record of monsoonal precipitation from northern Chile's Atacama Desert. Science 289 (5484), 1542–1546.
Bozkurt, D., Rondanelli, R., Garreaud, R., Arriagada, A., 2016. Impact of warmer eastern tropical Pacific SST on the March 2015 Atacama floods. Mon. Weather Rev. 144 (11), 4441–4460.
Brasher, B.R., Franzmeier, D.P., Valassis, V., Davidson, S.E., 1966. Use OF saran resin to coat natural soil clods for bulk-density and water-retention measurements. Soil Sci. 101 (2), 108.
Cabré, A., Remy, D., Aguilar, G., Carretier, S., Riquelme, R., 2020. Mapping Rain Storm Erosion Associated with an Individual Storm from InSAR Coherence-loss Validated by Field Evidence for the Atacama Desert: Earth Surface Processes and Landforms.
Cerling, T.E., 1984. The stable isotopic composition of modern soil carbonate and its relationship to climate. Earth Planet Sci. Lett. 71 (2), 229–240.
Cerling, T.E., Quade, J., 1993. Stable carbon and oxygen isotopes in soil carbonates: climate change in continental isotopic records, pp. 217–231.
Chávez, R., Moreira-Muñoz, A., Galleguillos, M., Olea, M., Aguayo, J., Latín, A., Aguilera-Betti, I., Muñoz, A., Manríquez, H., 2019. GIMMS NDVI time series reveal the extent, duration, and intensity of "blooming desert" events in the hyper-arid Atacama Desert, Northern Chile. Int. J. Appl. Earth Obs. Geoinf. 76, 193–203.
Cools, J., Vanderkimpen, P., El Afandi, G., Abdelkhalek, A., Fockedey, S., El Sammany, M., Abdallah, G., El Bihery, M., Bauwens, W., Huygens, M., 2012. An early warning system for flash floods in hyper-arid Egypt. Nat. Hazards Earth Syst. Sci. 12 (2), 443–457.
Coplen, T.B., Kendall, C., Hopple, J., 1983. Comparison of stable isotope reference samples. Nature 302 (5905), 236–238.
Corenblit, D., Baas, A.C.W., Bornette, G., Darrozes, J., Delmotte, S., Francis, R.A., Gurnell, A.M., Julien, F., Naiman, R.J., Steiger, J., 2011. Feedbacks between geomorphology and biota controlling Earth surface processes and landforms: a review of foundation concepts and current understandings. Earth Sci. Rev. 106 (3), 307–331.
Cosentino, N., Jordan, T., Derry, L., Morgan, J., 2015. 87Sr/86Sr in recent accumulations of calcium sulfate on landscapes of hyperarid settings: a bimodal altitudinal dependence for northern Chile (19.5° S–21.5° S). G-cubed 16 (12), 4311–4328.
Dane, J., Hopmans, J., 2002. Water retention and storage. In: Dane, J.H., Topp), G.C. (Eds.), Methods of Soil Analysis. Part 4. Soil Science Society of America, Madison, WI, USA. SSSA Book Series No. 5.
de Porras, M., Maldonado, A., Pol-Holz, D., Latorre, C., Betancourt, J., 2017. Late Quaternary environmental dynamics in the Atacama Desert reconstructed from rodent midden pollen records. J. Quat. Sci. 32 (6), 665–684.
Diaz, C., Wright, C., 1965. Soils of the Arid Zones of Chile. Food and Agriculture Organization of the United Nations.
Díaz, F.P., Latorre, C., Maldonado, A., Quade, J., Betancourt, J.L., 2012. Rodent middens reveal episodic, long-distance plant colonizations across the hyperarid Atacama Desert over the last 34,000 years. J. Biogeogr. 39 (3), 510–525.
Diederich, J.L., Wennrich, V., Bao, R., Büttner, C., Bolten, A., Brill, D., Buske, S., Campos, E., Fernández-Galego, E., Gödickmeier, P., 2020. A 68 Ka Precipitation Record from the Hyperarid Core of the Atacama Desert in Northern Chile: Global and Planetary Change, p. 103054.
Ebeling, A., Oerter, E., Valley, J., Amundson, R., 2016. Relict soil evidence for profound quaternary aridification of the Atacama Desert, Chile. Geoderma 267, 196–206.
Ewing, S., Macalady, J., Warren-Rhodes, K., McKay, C., Amundson, R., 2008a. Changes in the soil C cycle at the arid-hyperarid transition in the Atacama Desert. J. Geophys. Res.: Biogeosciences 113. G2.
Ewing, S.A., Michalski, G., Thiemens, M., Quinn, R.C., Macalady, J.L., Kohl, S., Wankel, S.D., Kendall, C., McKay, C.P., Amundson, R., 2007. Rainfall limit of the N cycle on Earth. Global Biogeochem. Cycles 21, 3.
Ewing, S.A., Sutter, B., Owen, J., Nishiizumi, K., Sharp, W., Cliff, S.S., Perry, K., Dietrich, W., McKay, C.P., Amundson, R., 2006. A threshold in soil formation at Earth's arid–hyperarid transition. Geochem. Cosmochim. Acta 70 (21), 5293–5322.
Ewing, S.A., Yang, W., DePaolo, D.J., Michalski, G., Kendall, C., Stewart, B.W., Thiemens, M., Amundson, R., 2008b. Non-biological fractionation of stable Ca isotopes in soils of the Atacama Desert, Chile. Geochem. Cosmochim. Acta 72 (4), 1096–1110.
Farr, T.G., Rosen, P.A., Caro, E., Crippen, R., Duren, R., Hensley, S., Kobrick, M., Paller, M., Rodriguez, E., Roth, L., 2007. The shuttle radar topography mission. Rev. Geophys. 45, 2.
Fick, A., 1855. Ueber diffusion. Ann. Phys. 170 (1), 59–86.
Finstad, K., Pfeiffer, M., Amundson, R., 2014. Hyperarid soils and the soil taxonomy. Soil Sci. Soc. Am. J. 78 (6), 1845–1851.
Finstad, K., Pfeiffer, M., McNicol, G., Barnes, J., Demergasso, C., Chong, G., Amundson, R., 2016. Rates and geochemical processes of soil and salt crust formation in Salars of the Atacama Desert, Chile. Geoderma 284, 57–72.
Finstad, K.M., Pfeiffer, M., McNicol, G., Tuite, M., Williford, K., Amundson, R., 2018. A late Quaternary paleoenvironmental record in sand dunes of the northern Atacama Desert, Chile. Quat. Res. 90, 127–138.
Freyer, D., Voigt, W., 2003. Crystallization and phase stability of CaSO 4 and CaSO 4–based salts. Monatshefte für Chemie/Chemical Monthly 134 (5), 693–719.
Gad-el-Hak, M., 2008. Large-scale Disasters: Prediction, Control, and Mitigation. Cambridge University Press.
Gajardo, R., 1994. La vegetación natural de Chile: clasificación y distribución geográfica.
Gamboa, C., Godfrey, L., Herrera, C., Custodio, E., Soler, A., 2019. The origin of solutes in groundwater in a hyper-arid environment: a chemical and multi-isotope approach in the Atacama Desert, Chile. Sci. Total Environ. 690, 329–351.
Garreaud, R., Rutllant, J., 1996. Análisis meteorológico de los aluviones de Antofagasta y Santiago de Chile en el periodo 1991-1993. Atmósfera 9 (4), 251–271.
Gayo, E.M., Latorre, C., Jordan, T.E., Nester, P.L., Estay, S.A., Ojeda, K.F., Santoro, C.M., 2012. Late Quaternary hydrological and ecological changes in the hyperarid core of the northern Atacama Desert (~ 21 S). Earth Sci. Rev. 113 (3), 120–140.
Gifford, G.F., Hawkins, R.H., 1978. Hydrologic impact of grazing on infiltration: a critical review. Water Resour. Res. 14 (2), 305–313.
Goudie, A.S., 2019. The History and Evolution of Desert Hydrology and Landforms: the Role of Climate Change, Dryland Ecohydrology. Springer, pp. 173–197.
Greenbaum, N., Ben-Zvi, A., Haviv, I., Enzel, Y., 2006. The hydrology and paleohydrology of the Dead Sea tributaries. GSA (Geol. Soc. Am.) Spec. Pap. (Reg. Stud.) 401, 63–93.
Hardie, L.A., 1967. The gypsum-anhydrite equilibrium at one atmosphere pressure. Am. Mineral. 52, 171–200.
Hillel, D., 1982. Introduction to Soil Physics. Academic Pres: İnc. San Dieoga, California, USA, p. 364.
Houston, J., 2002. Groundwater recharge through an alluvial fan in the Atacama Desert, northern Chile: mechanisms, magnitudes and causes. Hydrol. Process. 16 (15), 3019–3035.
Houston, J., 2006a. The great Atacama flood of 2001 and its implications for Andean hydrology. Hydrol. Process. 20 (3), 591–610.

Houston, J., 2006b. Variability of precipitation in the Atacama Desert: its causes and hydrological impact. Int. J. Climatol. 26 (15), 2181–2198.
Iguchi, T., Kozu, T., Meneghini, R., Awaka, J., Okamoto, K.i., 2000. Rain-profiling algorithm for the TRMM precipitation radar. J. Appl. Meteorol. 39 (12), 2038–2052.
James, A.N., 1992. Soluble Materials in Civil Engineering. Ellis Horwood.
Jordan, T., Riquelme, R., González, G., Herrera, C., Godfrey, L., Colucci, S., Gironás-León, J., Gamboa, C., Urrutia, J., Tapia, L., 2015. Hydrological and geomorphological consequences of the extreme precipitation event of 24-26 March 2015, Chile. In: Proceedings XIV Congreso Geológico de Chile.
Jordan, T.E., Herrera, C., Godfrey, L.V., Colucci, S.J., Gamboa, C., Urrutia, J., González, G., Paul, J.F., 2019. Isotopic characteristics and paleoclimate implications of the extreme rain event of march 2015 in northern Chile. Andean Geol. 46, 1.
Jordan, T.E., Kirk-Lawlor, N.E., Blanco, N.P., Rech, J.A., Cosentino, N.J., 2014. Landscape modification in response to repeated onset of hyperarid paleoclimate states since 14 Ma, Atacama Desert, Chile. Geol. Soc. Am. Bull. 126 (7–8), 1016–1046.
Jordan, T.E., Lohman, R.B., Tapia, L., Pfeiffer, M., Scott, C.P., Amundson, R., Godfrey, L., Riquelme, R., 2020. Surface materials and landforms as controls on InSAR permanent and transient responses to precipitation events in a hyperarid desert, Chile. Rem. Sens. Environ. 237, 111544.
Jungers, M.C., Heimsath, A.M., Amundson, R., Balco, G., Shuster, D., Chong, G., 2013. Active erosion–deposition cycles in the hyperarid Atacama Desert of Northern Chile. Earth Planet Sci. Lett. 371, 125–133.
Kim, S.-T., O'Neil, J.R., 1997. Equilibrium and nonequilibrium oxygen isotope effects in synthetic carbonates. Geochem. Cosmochim. Acta 61 (16), 3461–3475.
Latorre, C., Betancourt, J.L., Rylander, K.A., Quade, J., 2002. Vegetation invasions into absolute desert: a 45; th000 yr rodent midden record from the Calama–Salar de Atacama basins, northern Chile (lat 22°–24° S). Geol. Soc. Am. Bull. 114 (3), 349–366.
Luebert, F., Pliscoff, P., 2006. Sinopsis bioclimática y vegetacional de Chile. Editorial Universitaria.
Maldonado, A., Betancourt, J.L., Latorre, C., Villagran, C., 2005. Pollen analyses from a 50 000-yr rodent midden series in the southern Atacama Desert (25° 30′ S). J. Quat. Sci. 20 (5), 493–507.
Marinovic, S., Smoje, T., Maksaev, J., Hervé, A., Mpodozis, M., 1995. Hoja Aguas Blancas. Región de Antofagasta.
Marquet, P.A., Bozinovic, F., Bradshaw, G., Cornelius, C., Gonzalez, H., Gutierrez, J.R., Hajek, E.R., Lagos, J.A., Lopez-Cortés, F., Nunez, L., 1998. Los ecosistemas del desierto de Atacama y área andina adyacente en el norte de Chile. Rev. Chil. Hist. Nat. 71, 593–617.
May, S.M., Hoffmeister, D., Wolf, D., Bubenzer, O., 2019. Zebra stripes in the Atacama Desert revisited – granular fingering as a mechanism for zebra stripe formation? Geomorphology 344, 46–59.
May, S.M., Meine, L., Hoffmeister, D., Brill, D., Medialdea, A., Wennrich, V., Gröbner, M., Schulte, P., Steininger, F., Deprez, M., de Kock, T., Bubenzer, O., 2020. Origin and timing of past hillslope activity in the hyper-arid core of the Atacama Desert – the formation of fine sediment lobes along the Chuculay Fault System, Northern Chile. Global Planet. Change 184.
McDonnell, J.J., 1990. A rationale for old water discharge through macropores in a steep, humid catchment. Water Resour. Res. 26 (11), 2821–2832.
Medialdea, A., May, S.M., Brill, D., King, G., Ritter, B., Wennrich, V., Bartz, M., Zander, A., Kuiper, K., Hurtado, S., Hoffmeister, D., Schulte, P., Gröbner, M., Opitz, S., Brückner, H., Bubenzer, O., 2020. Identification of humid periods in the Atacama Desert through hillslope activity established by infrared stimulated luminescence (IRSL) dating. Global Planet. Change 185.
Melchiorre, E.B., Sickman, J.O., Talyn, B.C., Noblet, J., 2018. Isotope stratigraphy: insights on paleoclimate and formation of nitrate deposits in the Atacama Desert, Chile. J. Arid Environ. 148, 45–53.
Michalski, G., Böhlke, J., Thiemens, M., 2004. Long term atmospheric deposition as the source of nitrate and other salts in the Atacama Desert, Chile: new evidence from mass-independent oxygen isotopic compositions. Geochem. Cosmochim. Acta 68 (20), 4023–4038.
Morgan, A.M., Howard, A., Hobley, D.E., Moore, J.M., Dietrich, W.E., Williams, R.M., Burr, D.M., Grant, J., Wilson, S., Matsubara, Y., 2014. Sedimentology and climatic environment of alluvial fans in the martian Saheki crater and a comparison with terrestrial fans in the Atacama Desert. Icarus 229, 131–156.
Nester, P.L., Gayo, E., Latorre, C., Jordan, T.E., Blanco, N., 2007. Perennial stream discharge in the hyperarid Atacama Desert of northern Chile during the latest Pleistocene. Proc. Natl. Acad. Sci. U. S. A. 104 (50), 19724–19729.
Oerter, E.J., Amundson, R., 2016. Climate controls on spatial and temporal variations in the formation of pedogenic carbonate in the western Great Basin of North America. Geol. Soc. Am. Bull. 128 (7–8), 1095–1104.
Ortlieb, L., 1995. Eventos El Niño y episodios lluviosos en el desierto de Atacama: el registro de los últimos dos siglos. Bull. Inst. fr. études andines 24 (3), 519–537.
Owen, J.J., Amundson, R., Dietrich, W.E., Nishiizumi, K., Sutter, B., Chong, G., 2011. The sensitivity of hillslope bedrock erosion to precipitation. Earth Surf. Process. Landforms 36 (1), 117–135.
Owen, J.J., Dietrich, W.E., Nishiizumi, K., Chong, G., Amundson, R., 2013. Zebra stripes in the Atacama Desert: fossil evidence of overland flow. Geomorphology 182, 157–172.
Pfeiffer, M., Latorre, C., Santoro, C.M., Gayo, E.M., Rojas, R., Carrevedo, M.L., McRostie, V.B., Finstad, K.M., Heimsath, A., Jungers, M.C., De Pol-Holz, R., Amundson, R., 2018. Chronology, stratigraphy and hydrological modelling of extensive wetlands and paleolakes in the hyperarid core of the Atacama Desert during the late quaternary. Quat. Sci. Rev. 197, 224–245.
Placzek, C., Matmon, A., Granger, D., Quade, J., Niedermann, S., 2010. Evidence for active landscape evolution in the hyperarid Atacama from multiple terrestrial cosmogenic nuclides. Earth Planet Sci. Lett. 295 (1), 12–20.
Pliscoff, P., Luebert, F., Hilger, H.H., Guisan, A., 2014. Effects of alternative sets of climatic predictors on species distribution models and associated estimates of extinction risk: a test with plants in an arid environment. Ecol. Model. 288, 166–177.
Pueyo, J.J., Chong, G., Vega, M., 1998. Mineralogía y evolución de las salmueras madres en el yacimiento de nitratos Pedro de Valdivia, Antofagasta, Chile. Rev. Geol. Chile 25 (1), 03-15.
Quade, J., Rech, J.A., Latorre, C., Betancourt, J.L., Gleeson, E., Kalin, M.T., 2007. Soils at the hyperarid margin: the isotopic composition of soil carbonate from the Atacama Desert, Northern Chile. Geochem. Cosmochim. Acta 71 (15), 3772–3795.
Rech, J.A., Quade, J., Hart, W.S., 2003. Isotopic evidence for the source of Ca and S in soil gypsum, anhydrite and calcite in the Atacama Desert, Chile. Geochem. Cosmochim. Acta 67 (4), 575–586.
Retallack, G.J., 2005. Pedogenic carbonate proxies for amount and seasonality of precipitation in paleosols. Geology 33 (4), 333–336.
Ritter, B., Wennrich, V., Medialdea, A., Brill, D., King, G., Schneiderwind, S., Niemann, K., Fernández-Galego, E., Diederich, J., Rolf, C., 2019. Climatic fluctuations in the hyperarid core of the Atacama Desert during the past 215 ka. Sci. Rep. 9 (1), 5270.
Rondanelli, R., Hatchett, B., Rutllant, J., Bozkurt, D., Garreaud, R., 2019. Strongest MJO on record triggers extreme Atacama rainfall and warmth in Antarctica. Geophys. Res. Lett. 46 (6), 3482–3491.
Royer, D.L., 1999. Depth to pedogenic carbonate horizon as a paleoprecipitation indicator? Geology 27 (12), 1123–1126.
Schween, J.H., Hoffmeister, D., Löhnert, U., 2019. Filling the Observational Gap in the Atacama Desert with a New Network of Climate Stations: Global and Planetary Change, p. 103034.
Scott, C., Lohman, R., Jordan, T., 2017. InSAR constraints on soil moisture evolution after the March 2015 extreme precipitation event in Chile. Sci. Rep. 7.
Sepúlveda, S.A., Rebolledo, S., McPhee, J., Lara, M., Cartes, M., Rubio, E., Silva, D., Correia, N., Vásquez, J.P., 2014. Catastrophic, rainfall-induced debris flows in Andean villages of Tarapacá, Atacama Desert, northern Chile. Landslides 11 (3), 481–491.
Shen, H., Zheng, F., Wen, L., Lu, J., Jiang, Y., 2015. An experimental study of rill erosion and morphology. Geomorphology 231, 193–201.
SERNAGEOMIN, S. N. d. G. y. M., 2003. Mapa Geologico de Chile: version Digital. Base Geologica escala 1:1.000.000.
Shen, J., Shirey, T., Wyness, A., Claire, M., Zerkle, A., 2020. Spatial and Temporal Variability of Microbial Communities and Salt Distributions across an Aridity Gradient before and after Heavy Rains in the Atacama Desert: Prepints.
Smith, R.E., Goodrich, D.C., 2006. Rainfall Excess Overland Flow: Encyclopedia of Hydrological Sciences.
Stuut, J.-B.W., Lamy, F., 2004. Climate variability at the southern boundaries of the Namib (southwestern Africa) and Atacama (northern Chile) coastal deserts during the last 120,000 yr. Quat. Res. 62 (3), 301–309.
Sutter, B., Dalton, J., Ewing, S., Amundson, R., McKay, C., 2007. Terrestrial analogs for interpretation of infrared spectra from the Martian surface and subsurface: sulfate, nitrate, carbonate, and phyllosilicate-bearing Atacama Desert soils. J. Geophys. Res.: Biogeosciences 112. G4.
Tapia, L., Jordan, T., Riquelme, R., Herrera, C., Centella, K., Ramos, H., Venegas, M., 2015. Relación entre las distintas superficies y sus perfiles de humedad, post precipitaciones de marzo 2015, en la Sierra de Varas, II Región de Antofagasta, Chile. Proceedings Congreso Geológico Chileno 4.
Ugalde, P.C., Quade, J., Santoro, C.M., Holliday, V.T., 2020. Processes of Paleoindian site and desert pavement formation in the Atacama Desert, Chile. Quat. Res. 1–23.
Urrutia, R., Vuille, M., 2009. Climate change projections for the tropical Andes using a regional climate model: temperature and precipitation simulations for the end of the 21st century. J. Geophys. Res.: Atmosphere 114. D2.
Valdés-Pineda, R., Valdés, J.B., García-Chevesich, P., 2017. Modelación de Crecidas Aluvionales en la Cuenca del Río Copiapó, Chile. Ingeniería del agua 21 (2), 135–152.
Van Driessche, A., Benning, L., Rodriguez-Blanco, J., Ossorio, M., Bots, P., García-Ruiz, J., 2012. The role and implications of bassanite as a stable precursor phase to gypsum precipitation. Science 336 (6077), 69–72.
Van Genuchten, M.T., 1980. A closed-form equation for predicting the hydraulic conductivity of unsaturated soils. Soil Sci. Soc. Am. J. 44 (5), 892–898.
Van Genuchten, M.T., Leij, F., Yates, S., 1991. The RETC Code for Quantifying the Hydraulic Functions of Unsaturated Soils.
Vargas, G., Rutllant, J., Ortlieb, L., 2006. ENSO tropical–extratropical climate teleconnections and mechanisms for Holocene debris flows along the hyperarid coast of western South America (17–24 S). Earth Planet Sci. Lett. 249 (3), 467–483.
Voigt, C., Klipsch, S., Herwartz, D., Chong, G., Staubwasser, M., 2020. The Spatial Distribution of Soluble Salts in the Surface Soil of the Atacama Desert and Their Relationship to Hyperaridity: Global and Planetary Change, p. 184.
Wang, F., Ge, W., Luo, H., Seo, J.-H., Michalski, G., 2016. Oxygen-17 anomaly in soil nitrate: a new precipitation proxy for desert landscapes. Earth Planet Sci. Lett. 438, 103–111.
Wang, F., Michalski, G., Seo, J.-H., Granger, D.E., Lifton, N., Caffee, M., 2015.

Beryllium-10 concentrations in the hyper-arid soils in the Atacama Desert, Chile: implications for arid soil formation rates and El Niño driven changes in Pliocene precipitation. Geochem. Cosmochim. Acta 160, 227–242.
Wang, Y., McDonald, E., Amundson, R., McFadden, L., Chadwick, O., 1996. An isotopic study of soils in chronological sequences of alluvial deposits. Providence Mountains, California: Geol. Soc. Am. Bull. 108 (4), 379–391.
Warren-Rhodes, K.A., Rhodes, K.L., Pointing, S.B., Ewing, S.A., Lacap, D.C., Gómez-Silva, B., Amundson, R., Friedmann, E.I., McKay, C.P., 2006. Hypolithic cyanobacteria, dry limit of photosynthesis, and microbial ecology in the hyperarid Atacama Desert. Microb. Ecol. 52 (3), 389–398.
Weiler, M., McDonnell, J., 2004. Virtual experiments: a new approach for improving process conceptualization in hillslope hydrology. J. Hydrol. 285 (1), 3–18.
Weiler, M., McDonnell, J.J., Tromp-van Meerveld, I., Uchida, T., 2005. Subsurface Stormflow: Encyclopedia of Hydrological Sciences.
Wheater, H.S., 2002. Hydrological processes in arid and semiarid areas: hydrology of wadi systems. IHP-V, Technical documents in hydrology 55, 5–22.
Wilcox, A.C., Escauriaza, C., Agredano, R., Mignot, E., Zuazo, V., Otárola, S., Castro, L., Gironás, J., Cienfuegos, R., Mao, L., 2016. An integrated analysis of the March 2015 Atacama floods. Geophys. Res. Lett. 43 (15), 8035–8043.
Yair, A., Lavee, H., 1985. Runoff generation in arid and semi-arid zones: hydrological forecasting/. MG Anderson and TP Burt.
Zhang, R., 1997. Determination of soil sorptivity and hydraulic conductivity from the disk infiltrometer. Soil Sci. Soc. Am. J. 61 (4), 1024–1030.
Zomer, R.J., Trabucco, A., Bossio, D.A., Verchot, L.V., 2008. Climate change mitigation: a spatial analysis of global land suitability for clean development mechanism afforestation and reforestation. Agric. Ecosyst. Environ. 126 (1), 67–80.